NON-LOCAL EFFECTS OF ANTIBIOTIC RESISTANCE CAUSING MUTATIONS REVEAL AN ALTERNATIVE REGION FOR TARGETING ON FTSW/PENICILLIN BINDING PROTEIN 3 COMPLEX OF *H. INFLUENZAE*

A THESIS SUBMITTED TO
THE GRADUATE SCHOOL OF
ENGINEERING AND NATURAL SCIENCES
OF ISTANBUL MEDIPOL UNIVERSITY
IN PARTIAL FULFILLMENT OF THE REQUIREMENTS FOR
THE DEGREE OF
MASTER OF SCIENCE
IN
BIOMEDICAL ENGINEERING AND BIOINFORMATICS

By

Almotasem Belah Alhamwi

January, 2023

NON-LOCAL EFFECTS OF ANTIBIOTIC RESISTANCE CAUSING MUTATIONS REVEAL AN ALTERNATIVE REGION FOR TARGETING ON FTSW/PENICILLIN BINDING PROTEIN 3 COMPLEX OF *H. INFLUENZAE*

By Almotasem Belah Alhamwi

23 January 2023

We certify that we have read this dissertation and that in our opinion it is fully adequate, in scope and in quality, as a dissertation for the degree of Master of Science.

Assist. Prof. Özge Şensoy (Advisor)

Prof. Canan Atılgan (Co-Advisor)

Assist. Prof. Kıvanç Kök

Prof. Süleyman Yıldırım

Prof. Mine Yurtsever

Approved by the Graduate School of Engineering and Natural Sciences:

Prof. Yasemin Yüksel Durmaz
Director of the Graduate School of Engineering and Natural Sciences

I hereby declare that all information in this document has been obtained and presented in accordance with the academic rules and ethical conduct. I also declare that, as required by these rules and conduct, I have fully cited and referenced all material and results that are not original to this work.

Signature :

Name, Surname: ALMOTASEM BELAH ALHAMWI

ACKNOWLEDGEMENT

Words cannot express my gratitude to my advisor Assis. Prof. Özge ŞENSOY for her patience, support, generous knowledge, and guidance. Her supervision was one of the reasons which encouraged me to keep up with my journey and achieve my goals. Additionally, I would like to express my deepest appreciation to my co-advisor Prof. Canan Atilgan for her continuous inspiration and motivation.

I would like to extend my sincere thanks to the director of the Graduate School of Engineering and Natural Sciences (GSENS) Prof. Yasemin YÜKSEL DURMAZ for being there whenever I need her guidance. I am also thankful to my thesis defense committee for their valuable contribution.

Thanks should also go to all members of Şensoy's Computational Biophysics Lab who supported and generously share their knowledge with me.

Lastly, I could not have undertaken this journey without my family and my friends – who became a part of my family. Their belief in me and their emotional support had kept me up all the time, motivated, and wanted to do my best.

Almotasem Belah Alhamwi

January, 2023

CONTENTS

Page

LIST OF FIGURES

LIST OF TABLES

LIST OF SYMBOLS

ε_{ij} :Well-depth value
σ :LJ parameter
ε_{rel} :Relative dielectric constant
φ_a :Angle
θ_d :Dihedral angle
θ_{id} :Improper dihedral angle
V_b :Bonded potential
V_a :Angle potential
V_d :Dihedral potential
V_{id} :Improper Dihedral potential

ABBREVIATIONS

AMR	:Antimicrobial Resistance
PBP	:Penicillin-Binding Protein
PBP3	:Penicillin-Binding Protein 3
HMW	:High Molecular Weight
LMW	:Low Molecular Weight
SEDS	:Shape, Elongation, Division, and Sporulation
TM	:Transmembrane Domain
N-t	:N-terminal periplasmic modulus domain
TP	:Transpeptidase Domain
H.influenzae	:*Haemophilus influenzae*
NTHi	:*nontypeable H. influenzae*
Hib	:*H.influenzae type b*
Low-r	:Low Resistance
Medium-r	:Medium Resistance
High-r	:High Resistance
CM	:Cytoplasmic Membrane
OM	:Outer Membrane
AA	:All-atom
MD	:Molecular Dynamics
QM	:Quantum Mechanics
CG	:Coarse-grained
LJ	:Lennard-Jones
3D	:Three-dimensional
PDB	:Protein Data Bank
OPM	:Orientations of Proteins in Membranes

H.İNFLUENZA'YA AİT FTSW/PENİSİLİN BAĞLAYAN PROTEİN 3 KOMPLEKSİNDE BULUNAN VE ANTİBİYOTİK DİRENCİNE NEDEN OLAN MUTASYONLARIN ALTERNATİF HEDEF BÖLGELER AÇIĞA ÇIKARMASI

ÖZET

Almotasem Belah Alhamwi

Biyomedikal Mühendisliği ve Biyoinformatik, Yüksek Lisans

Tez Danışmanı: Dr. Öğr. Üyesi Özge Şensoy

Eş Danışman: Prof. Dr. Canan Atılgan

Ocak, 2023

Halihazırda reçetelenen antibiyotikler, ağırlıklı olarak yabanıl proteinlerin katalitik bölgesini hedeflemektedir. Bununla beraber, yaşadıkları zorlu çevre koşullarına ayak uydurabilmek için bakteriyel proteinlerin katalitik bölgesinde ve/veya civarında bulunan amino asitlerde mutasyon meydana gelir. Sonuç olarak, bu durum, bakterilerde antibiyotik direncinin ortaya çıkmasına neden olur. Dünya Sağlık Örgütü'nün 2022 yılında yayımladığı rapora göre, antibiyotik direnci gösteren bakteriler yıllık olarak 4.95 milyon kişinin ölümüne sebep olmaktadır. Bundan dolayı, şu ana kadar ağırlıklı olarak hedeflenen ve dirence neden olan bakteriyel proteinlerin katalitik bölgesine alternatif bölgelerin belirlenebilmesi önem taşımaktadır. Bu da hedef sistemin dinamiği hakkında bilgi sahibi olunmasını gerektirmektedir. Bu doğrultuda, yüksek seviyede antibiyotik direncine neden olduğu deneysel çalışmalarla belirlenmiş, S385T + L389F + N526K üçlü mutasyon setinin, dirençli organizmalar gruplandırılmasında, öncelikli grupta bulunan ve dirençli bir patojen olan *H. influenzae* üzerindeki etkisi hesaplamalı metotlar yardımıyla irdelenecektir. Bu çalışma kapsamında, hücre duvarının sentezini engelleyebilen β-laktam antibiyotiklerine karşı dirençli olan, penisilin bağlayıcı protein 3 (PBP3) ve bu proteinin FtsW proteini ile yaptığı kompleks kullanılacaktır.

Elde edilen sonuçlar, mutasyonların, PBP3 üzerinde, hem lokal hem de global etkiye sahip olduğunu göstermiştir. Bu etkiler, FtsW/PBP3 kompleksi için daha belirgindir. Lokal etkiler kapsamında, PBP3'nin, transpeptidaz domaini üzerinde bulunan aktif bölgesini çevreleyen β-yaprak yapılarının membrana göre yönlenmesinin etkilendiği gözlemlenmiştir. Öyleki, mutant PBP3'de, proteinin aktif bölgesi, periplazmik bölgeye doğru yönlenmiştir. Ayrıca, proteinin katalizinde önemli role sahip olduğu bilinen gatekeeper ve β3-β4 loop yapılarının oynaklığının, mutant FtsW/PBP3 kompleksinde arttığı gözlemlenmiştir. Bunun dışında, global etkiler kapsamında, pedestal domainin, özellikle çatal yapısının açıklığının, yabanıl ve mutant proteinde farklılık gösterdiği gözlemlenmiştir. Mutant FtsW/PBP3 kompleksinde, çatal yapısı hem açık hem de kapalı şekilde bulunabilirken, yabanıl komplekste, yalnızca açık form tercih edilmiştir. Ayrıca, çatal açıklığının, β-yaprak yapısının yönlenmesine göre farklılık gösterdiği gözlemlenmiştir. Öyleki, β-yaprak, membrana parallel olarak yönlendiğinde, çatalın kapalı forma, dik olarak yönlendiğinde ise çatalın açık forma adapte olduğu gözlemlenmiştir. İlginç bir

şekilde, mutant komplekste, çatal kapalı formdayken, N-terminal periplazmik modül (N-t) ile transpeptidaz domaini (TP) arasında olduğu düşünülen allosterik etkileşim şebekesine daha çok amino asit katkıda bulunmaktadır. Son olarak, çatalın kapalı forma uyum sağladığı durumda, β-lactam antibiyotiklerinden olan sefiksime karşı olan bağlanma eğiliminin daha yüksek olduğu gözlemlenmiştir. Tüm bu sonuçlar, mutant PBP3'de, çatalın kapalı formunu stabilize edebilen küçük terapötik moleküllerin, antibiyotik direnç problemine alternatif bir yaklaşım sunma potansiyelinin olduğunu düşündürmektedir.

Anahtar sözcükler: Dirençli Bakteriler, Penisilin bağlayıcı protein 3, *Haemophilus influenzae*, β-laktam antibiyotikler.

NON-LOCAL EFFECTS OF ANTIBIOTIC RESISTANCE CAUSING MUTATIONS REVEAL AN ALTERNATIVE REGION FOR TARGETING ON FTSW/PENICILLIN BINDING PROTEIN 3 COMPLEX OF *H. INFLUENZAE*

ABSTRACT

Almotasem Belah Alhamwi

MSc in Biomedical Engineering and Bioinformatics

Advisor: Assist. Prof. Özge Şensoy

Co-Advisor: Prof. Canan Atılgan

January, 2023

Currently prescribed antibiotics predominantly target the catalytic site of wild type bacterial proteins; however, bacteria adopt mutations in/around this site to survive in their challenging environment, which eventually leads to the emergence of resistant bacteria. Since resistant bacterial infections cause annually 4.95 million deaths as reported by the World Health Organization (2022), there is urgent need for identifying alternative drug binding regions on resistance-causing proteins, which requires knowledge of the dynamics of the system. Towards this end, we set out to investigate the impact of a high-resistance causing triple mutation (S385T + L389F + N526K) on the dynamics of a prioritized resistant pathogen, *H. influenzae*, by computational techniques. We focused on penicillin-binding protein 3 (PBP3) and its complex with FtsW, which display resistance towards β-lactam antibiotics that prevent bacterial cell wall synthesis. We showed that mutations had both local and non-local effects on PBP3, and these were amplified in the FtsW/PBP3 complex. In terms of local effects, the orientation of the β-sheet, which surrounds the active site of PBP3 located on the transpeptidase domain was impacted such that the catalytic site of the mutant enzyme became exposed towards the periplasmic region. In addition, the flexibility of the $\beta3$-$\beta4$ loop, which was shown to modulate the catalysis of the enzyme, increased in the mutant FtsW/PBP3 complex. As to the non-local effects, the dynamics of the pedestal domain (N-terminal periplasmic modulus (N-t)), in particular the opening of the fork, was different between the wild type and the mutant enzyme. Both open and closed forms of the fork were adopted in the mutant FtsW/PBP3, whereas only the open form was preferred in the wild type complex. We also demonstrated that the opening of the fork was modulated by the orientation of the β-sheet such that the open form was adopted when the β-sheet was aligned perpendicular to the membrane, whereas the closed fork was adapted when the β-sheet was aligned parallel to it. Interestingly, we found that the closed fork caused a higher number of residues to participate in the hypothesized allosteric communication network that connects the N-terminal periplasmic modulus (N-t) to the transpeptidase domain (TP) in the mutant enzyme. Finally, we demonstrated that the closed fork conformation results in a more favorable binding energy with the β-lactam antibiotics, particularly cefixime, suggesting that small therapeutics molecules that can stabilize the closed fork conformation of the mutant PBP3 may pave the way for more effective ways to combat resistant bacteria.

Keywords: Resistant Bacteria, Penicillin-binding Protein 3, *Haemophilus influenzae*, *β*-lactam Antibiotics.

CHAPTER 1

1. INTRODUCTION

The canonical strategy for developing antibiotics has been targeting the catalytic sites of proteins which are responsible for mediating metabolic activities of bacteria including replication and cell wall synthesis [1], [2]. Due to the challenges associated with de novo design, higher-generation antibiotics have been developed where a core scaffold is substituted by complex functional groups at each generation [3]. In that way, it has been proposed that bacteria would not recognize the scaffold that is shielded, and the resistance would be prevented; however, this strategy does not work out as planned, since bacteria develop novel strategies to resist these antibiotics, which has consequently led to the emergence of more severe antibiotic resistance [4].

Another level of complexity associated with currently prescribed antibiotics is that they are designed to target wild type bacterial proteins; however, these biological catalysts continuously undergo mutations, in particular, within/around their catalytic sites, as they reside in a very challenging environment [5], [6]. As an alternative strategy, allosteric regions, other than the catalytic sites can be identified, which can be targeted by therapeutics for modulating function of the mutant protein. This alternative strategy requires developing a holistic understanding of the interaction network of the protein at the molecular-level [7].

Among the proteins that have been targeted for antibiotic development purposes, penicillin-binding protein 3 (PBP3) of *Haemophilus influenzae (H.influenzae)* has been singled out. *H.influenzae* has been categorized under the prioritized pathogens according to the World Health Organization Report (2022). PBPs, which are classified under the serine acyltransferase enzyme family, are responsible for synthesizing the major component of the inner cell membrane, peptidoglycan [8], [9]. They are broadly classified into two groups: high molecular weight (HMW) and low molecular weight (LMW). Class B PBPs

are members of the former group and they are monofunctional enzymes responsible only for transpeptidase activities, whereas Class A are members of the latter group which also perform transglycosylase activities. PBP3 of *H.influenzae* is a categorized under Class B HMW PBPs [10], [11].

The PBP3 of *H.influenzae* consists of three domains, namely, transmembrane domain (TM), N-terminal periplasmic modulus domain (N-t), and transpeptidase domain (TP) (See **Figure 1.1**), each of which is devoted to a specific function. For instance, TM is involved at the interface formed with FtsW, which acts as a peptidoglycan polymerase. The N-t, although poorly crystallized, is thought to, *i*) mediate interactions with divisome/elangosome partners, *ii*) enhance the enzymatic activity of TP, and *iii*) modulate allosteric communication between the domains [8], [12]–[14], yet the molecular mechanism remains elusive. Lastly, the TP is responsible for the catalytic activity of the protein and also acts as the penicillin-binding domain which is conserved among class A and B PBPs. Certain mutations occurring in the TP have been shown to be responsible for development of antibiotic resistance. For instance, N526K mutation causes low antibiotic resistance (Low-rPBP3) towards β-lactam antibiotics, whereas additional S385T (Medium-rPBP3) and L389F mutations further increase the resistance (High-rPBP3). Understanding the impact of these mutations on structure and dynamics of PBP3 at the molecular level will aid the development of more effective therapeutics to combat resistant bacteria [15], [16]. For this purpose, we investigated the impact of the high resistance-causing triple mutation on the dynamics of FtsW-PBP3 complex in *H.influenzae*, which is involved in the divisome and elongasome, by means of computational tools against the background of both the low-resistance single mutant and the wild type protein. We showed that the mutation impacted orientation of the active site of PBP3 with respect to the membrane and also the opening of the fork located on the N-t domain. Moreover, the opening of the fork was shown to dictate the number of residues participating in the proposed allosteric network that connects the N-t to the catalytic site. Lastly, covalent docking calculations showed that the binding affinity of antibiotics and peptidoglycan substrate (D-alanyl-D-alanine) was lower in the mutant PBP3 than in the wild type enzyme.

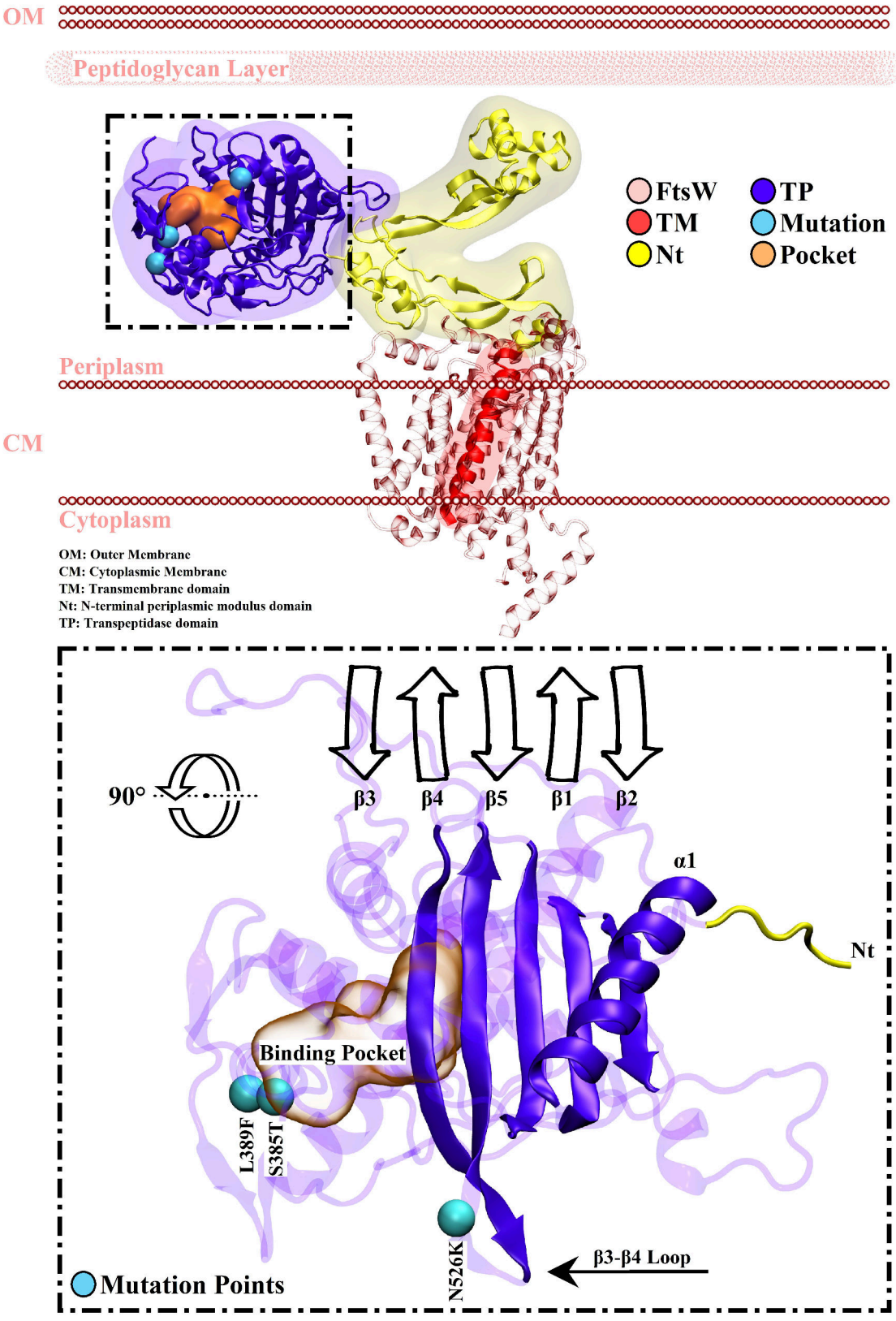

Figure 1.1: Schematic representation of the 3D structure of FtsW-PBP3 complex is shown in surface and new cartoon representation. The outer membrane (OM) and the peptidoglycan layer were not included in the molecular dynamics simulations but they are shown here for presentation of the membrane of gram-negative bacteria. Water and phospholipids are not shown for the sake of simplicity. The TP domain is shown in detail in the lower panel along with the binding pocket and the positions of the mutated residues.

CHAPTER 2

2. THEORETICAL PART

2.1. Bacterial Infection Therapy: Antibiotics and Antibiotic Resistance

Antibiotics are named the wonder medicines developed to fight infections caused by bacteria [17]. Cellular growth, replication, elongation, sporulation, and survival are the aim of all living organisms. Toward this end, bacteria use their genetic immune defense reaction in the presence of drugs (antibiotics) to assure their continued existence and this is assumed to be the natural way of developing "resistance" [18]. On the other hand, There are external factors that enhance the resistance development such as (mis/over) use of antibiotics, misleading prescription, contamination in the hospitals/clinics, and insufficient personal hygiene [19]–[21]. In addition, the development rate of new antibacterial agents plays a key role in the war against superbugs.

Besides genetic natural resistance, bacteria might acquire the resistance by translating, conjugating, or transporting resistance genes and/or alternations (mutations) in the DNA [22], [23]. The mechanism is categorized into four groups: *i*) limiting the drug uptake, *ii*) modifying the drug target, *iii*) inactivating the drug, and *iv*) extruding (efflux) the drug outside the cell. Gram-negative bacteria are more likely to limit drug uptake compared to gram-positive bacteria because they have a double cell membrane and intrinsic lower permeability. Moreover, modifying the drug target is a well-known mechanism that rearranges and/or alters the antibiotic target. Alternations (mutations) in penicillin-binding proteins (PBPs), which are the β-lactam antibiotics target, is one of the documented examples under the present category. Nevertheless, the drug itself might be inactivated by a chemical group transfer or enzymatic structural distortion via β-lactamases. Acetyl, phosphoryl, and adenyl are all possible chemical groups that can be transferred to prevent the binding between the drug and its target [24]. Nevertheless, bacteria are able to resist the

treatment by transporting the agent outside the cell by overexpressing the efflux pump proteins [25].

β-lactam antibiotics, the most used commercial antibacterial agents worldwide, are decreasing the bacterial cell rigidity and cause cell lysis by targeting the synthesis of a major cellular component called "peptidoglycan" [26], [27]. Peptidoglycan is a mesh-like structure composed of glycan strands connected by short peptides that maintain the shape of bacterial cells. Its synthesis is initiated at the cytoplasmic site by producing the lipid II precursor molecule that is flipped to the periplasmic site where polymerization and cross-linking of the new glycan strand take place [28]. Gram-positive bacteria have multilayered peptidoglycan (10 to 40 layers) while gram-negative might have one or two layers [29].

2.2. PBPs (Penicillin-Binding Proteins) and SEDS (Shape, Elongation, Division, and Sporulation)

PBPs are enzymes responsible for polymerizing (glycosyltransferase) and cross-linking (transpeptidase) the glycan strands. In addition, some of them might perform a reverse enzymatic activity and hydrolyze the peptide bond between two glycan strands (endopeptidase). They have two main categories: high molecular mass (HMM) and low molecular mass (LMM). The members of the former category are multimodular key players in peptidoglycan synthesis [8]. Moreover, their main structure is studied to consist of a cytoplasmic tail, a transmembrane helix, and two connected domains on the periplasmic space. The domain that comes after the transmembrane helix (N-terminal periplasmic domain) distinguishes class A and class B HMM PBPs. In class B, it was assigned to non-enzymatic activities whereas in class A it exhibits catalyzing the elongation of a synthesized glycan strand. The other periplasmic domain is responsible for cross-linking the polymerized glycan strands to the existing mesh, and it is called the penicillin-binding domain as it binds to β-lactam antibiotics. Additionally, it is also known as transpeptidase domain due to its enzymatic reactivity. It consists of five core stranded β-sheet surrounded by a number of α-helices. Contrary to the N-terminal domain, penicillin-binding domain is well-conserved among PBPs classes, and it has three motifs that form the catalytic pocket and are involved in the interaction with the substrate: S(active site)XXK, SXN, and KTG. It is worth to be mentioned that the number of PBPs depends on the microorganism, *Escherichia coli* has 12 PBPs, *Haemophilus influenzae* has 8 PBPs, and

Neisseria gonorrhoeae has 4 PBPs [30], [31].

For decades, Class A PBPs are assumed the only enzymes responsible for polymerizing glycan strands (glycosyltransferase) [10]. However, recently, the shape, elongation, division, and sporulation (SEDS) proteins family has been introduced with broader structural conservation [32]. RodA and FtsW are members of this family, playing a key role in cell elongation and division, respectively. In the absence of RodA, bacteria are still able to grow, whereas the presence of FtsW is essentially required for septal cell wall assembly [33]–[35]. They consist of 10 transmembrane helix segments which are supposed to transport the lipid II precursor molecule across the cytoplasmic membrane [36]–[38]. Consequently, RodA-PBP2/FtsW-PBP3 complex working principle is explained by accommodating Lipid II molecule from the cytoplasmic site, then polymerizing and cross-linking a new glycan strand. It is to be noted that, RodA/FtsW is requiring its bPBP partner to exhibit glycosyltransferase activities, while PBP2/PBP3 is able to transpeptidase glycan strands that were polymerized by other glycosyltransferases [35].

Sjodt et al introduced the structures of RodA and RodA-PBP2 complex from *Thermus thermophilus*. Comparing the isolated structure with the complex one, the seventh transmembrane helix segment (TM7) of RodA shows a shift of approximately 10Å. This shift formed a membrane-accessible cavity with 15Å width and 30Å height that is proposed to accommodate Lipid II precursor molecule. However, the complex structure reveals two main interfaces I and II. Interface I is hydrophobically formed between the transmembrane helix of PBP2 and transmembrane segments 8 (TM8) and 9 (TM9) of RodA within the membrane plane. It is proposed to provide most of the required energy for the complex formation. On the other hand, interface II involved three β-sheets and a small loop of the N-terminal periplasmic domain of PBP2 which interact with the extracellular loop (ECL4) of RodA. The complex adopts a conformation that extends only 45Å above the cytoplasmic membrane, while the peptidoglycan layer of gram-negative bacteria is located 120Å away from the membrane. Accordingly, the complex is assumed to sample a wide range of conformations that allow adopting “compact” and “extended” states, each of which locates PBP2 45Å and 100Å away from the membrane, respectively. Compact conformation is required for the allosteric activation of RodA and initiation of polymerization, whereas extended conformation allows PBP2 to attach the polymerized strand to the existing layer. The precise regulation of those conformations is essentially required to avoid

a toxic peptidoglycan synthesis cycle, thus, cellular survival [13], [39].

Divisome and elongasome (Rod system) are multi-protein complexes that regulate bacterial cell division and elongation, respectively, thus modulating peptidoglycan synthesis [28]. The signaling cascade of those complexes, although poorly identified, indicates that RodA/FtsW and PBP2/PBP3 are late-stage contributors in the peptidoglycan synthesis [40]. Accordingly, RodA-PBP2 or FtsW-PBP3 complexes acquire an activation signal to start their activities. MreC, a bitopic protein that has a large periplasmic domain with a butterfly-like architecture, is documented to interact with the N-terminal periplasmic (pedestal) domain of PBP2 and activate the complex [41]. *Martins et al.* reported that the recognition of MreC requires opening of the N-terminal periplasmic domain of bPBP. In addition, they defined two modes of peptidoglycan biosynthesis "on" and "off". In the former, the N-terminal periplasmic domain adopts "open" conformation and the MreC-PBP2 complex is formed, while in the latter, MreC interacts with other partners. MreD is one of the proposed partners which has an additional impact on conformations sampled by PBP2 [41].

2.3. Gram-negative Pathogens, In Particular *Haemophilus influenzae*, Resistance Development Mechanism

H. influenzae is a gram-negative pathogen that has two types according to the presence/absence of polysaccharide capsule: encapsulated with six more sub-categories (a-f) and nonencapsulated (nontypeable) [42]. It can target different parts of the human body and cause various diseases such as nervous system (meningitis), respiratory tract (pneumonia), auditory system (acute otitis media), and cardiovascular system (bacteremia). Mucosal-associated infections are mostly caused by *nontypeable H. influenzae (NTHi)* as it adheres to mucus or cells' surfaces of the upper airway [43], [44]. Nevertheless, *H. influenzae type b (Hib)* was recording annual deaths rate of 386.000 till the introduction of polysacharide-protein conjugate vaccines [45].

β-lactam antibiotics with different generations, doses, and combinations are used to treat *H. influenzae* infections. However, PBP3-mediated resistance that is encoded by *ftsI* gene is increasing worldwide [46]. PBP3 is acquiring mutations at different points in its penicillin-binding (transpeptidase) domain, particularly, around SSN and KTG motifs. M377, S385, L389, R517, and N526 are mutation points that develop various levels

of resistance according to their combination. R517H and N526K are mutually exclusive mutations that cause low-resistance levels [47]; however, adding M377I, S385T, and/or L389T further increases the level to medium- and high-resistance. For instance, *Hasegawa et al.* defined two groups of β-lactamase nonproducing ampicillin resistant *H. influenzae* named low-resistant and resistant which has R517H/N526K and S385T+(R517/N526) in their PBP3, respectively [48]. Additionally, *Skaare et al.* introduced two high-resistant groups that acquire S385T+(R517/N526) in the presence/absence of L389F [15], [16].

In bPBP, β3 strand and β3-β4 loop catalyze the acylation reaction by twisting and sampling favorable conformational changes, respectively. Mutations near the KTG motif are introduced in the β3-β4 loop region, suggesting that it hinders the flexibility and lowers the binding affinity toward antibacterial agent by fixing the loop's state [49]. However, although poorly understood, resistance mutations ought to *i*) decrease the acylation rate, *ii*) increase the deacylation rate, *iii*) reduce the binding affinity toward antibiotics or combine more than one of the mentioned impacts [50]. *Fenton et al.* define two conformations of β3-β4 loop namely "extended" and "twisted" with suggested low- and high-binding affinity toward ceftriaxone [51], respectively. In PBP2 of *Neisseria gonorrhoeae*, wild type enzyme was sampling both conformations in an equal ratio whereas the resistant enzyme sampled the extended conformation more preferably. It is also important to mention that, in a recent crystal structure, the twisted conformation is found only in the acyl-complex enzyme, not in the *apo* form [52]. Nevertheless, the extended state is supposed to facilitate the peptidoglycan substrate entry which considerably requires a larger binding surface area compared to a cephalosporin antibiotic. Consequently, the transition between extended and twisted states is essential for peptidoglycan synthesis and transpeptidase activity [51].

Other gram-negative bacteria such as *Escherichia coli*, *Caulobacter crescentus*, and *Thermus thermophilus* are able to acquire mutations in the extracellular loop (ECL4) of their SEDS proteins. In addition, they might have alternations in the pedestal domain of the bPBP partner. Accordingly, the complex interaction (interface II) is disturbed and the activation pathway is accessed. Some of those mutations are proposed to change the phenotype to inactive/hyperactive according to the amino acid conservation among the microorganisms. For instance, in RodA of *E. coli*, A234T is a highly conserved mutation that causes hyperactive division phenotype and mapped to be located at residue number 227 of *T. thermophilus*. Hyperactive phenotype is supposed to bypass its elongasome

partner-trigger signal [53].

2.4. Computational Methods and Approaches

2.4.1. Homology modeling and protein structures prediction methods

Homology modeling is a structure prediction computational tool that aims to predict the three-dimensional (3D) structure of a macro-molecule based on its amino acid sequence and a homologous template. The main concern is to model the structure with an accuracy matches the best achieved experimental results. It is worth to be mentioned that, experimental techniques such as NMR and X-ray diffraction might fail to crystallize some of the structures due to different reasons, hence, the only way to obtain structural information is the models. Since similar sequences tend to fold into similar/identical structures, the number of aligned residues versus the percentage of identical residues is exponentially correlated and detects the model accuracy. Homology modeling steps can be summarized in practice as follow: recognizing the template and aligning the sequences, correcting the alignment, generating the backbone, modeling the loops regions, modeling the side chains, optimizing the model, and finally validating the model. The sequence alignment and correction are based on generating a residue exchange matrix that has x- and y-axises of the target and the selected template sequences. The values of the matrix depend on the alignment criteria. For instance, the similarity in properties of amino acids might (or might not) be taken into consideration, thus, the scoring criteria is changing accordingly. To find the best alignment between two sequences, the optimum path is found. Additionally, during the alignment correction, the target sequence ought to be divided into chunks and different templates can be used to find the optimum structure, a step that is named "multiple sequence alignment". Furthermore, building up backbone and side chains concerns the identity between the two residues, if they are identical, the coordinates of backbone and side chain are copied, if not, the coordinates of backbone only are copied. The loop regions modeling is done to fill out the gaps in the model based on one of two approaches: searching on PDB for similar loops that have the same endpoints or using *ab initio* fold prediction. However, similar to the former approach, modeling the side chains is based on conserved rotamers library searching. Model optimization and validation are energy-based calculations used the assigned force field parameters. It is to be noted, homology modeling depends solely on the user's choices in each individual step, starting from the

templates selection to the force field determination [54]–[59].

Nowadays, protein structures, folding, and interactions prediction methods are continuously developed to determine high-accuracy outputs. *Baek et al.* introduce a deep-learning based method "RoseTTAFold" [60] that uses neural network analysis to predict protein structures. Besides, the method provides insight into the unknown structure proteins' functions and it can develop protein-protein complex models. It shows high accuracy and rapid model generation as its comparatives do (AlphaFold [61], [62]).

2.4.2. Molecular dynamics (MD) simulations

The Quantum nature of nuclei and electrons is represented by a numberless of biological events such as electrons rearrangement in biochemical reactions, tunneling of electrons and protons, and coupled proton-electron transfers. Consequently, Quantum Mechanical (QM) phenomenon is the core of various biological events including respiration, photosynthesis, sensory, and taste. However, describing such processes needs to consider a high number of atoms (up to 100.000 atoms/molecule) and long time scales (longer than a second in certain cases), hence, requiring unachievable computations once represented with QM calculations [63], [64].

In the late 1970s [65], molecular dynamics (MD) simulations are introduced with a set of approximations and assumptions that reduced the calculations' complexity. To run MD simulations, the three-dimensional structure is needed either crystallized experimentally or predicted by modeling techniques. Thereafter, the forces acting on each atom of the system are estimated concerning bonded and non-bonded interactions. The bonded interactions consider distances between two points (bonds), angles formed by three points (angles), and angles formed by four points (dihedrals) whilst the non-bonded concern van der Waals and electrostatic interactions, each of which is modeled by Lennard-Jones 6-12 potential and Coulomb's law respectively [66], [67]. The aforementioned terms are parameterized to fit the real molecule motion with help of a "force field", a collection of parameters describing the impact of each atomic force on the simulated system. CHARMM, AMBER, and GROMOS are all well-known force fields used in MD simulations [68]–[71]. Furthermore, once the forces calculations are performed, positions of the system's atoms are detected based on solving Newton's equations of motion. Assigning the initial velocities to each atom is required to initiate the repeating loop of solving the equations

and detecting the displaced atom position.

2.4.3. Coarse-grained (CG) molecular dynamics (MD) simulations

Coarse-grained (CG) molecular dynamics (MD) simulations have been widely used to simulate large and complex systems. It can simplify the all-atom (AA) representation, lower the resolution, speed up the dynamics, and access larger time scales. All-atom (AA) molecular dynamics (MD) simulations when used for complex systems demand computations and ought to access limited time scales. Implicit solvent models are introduced as alternatives to explicit models to deal with the limitations. However, they failed to capture solute-solvent interactions; consequently, were used only when such details are not essentially required. CG-MD are used for proteins, peptides, and metals systems. In particular, they are well-known to study protein/peptide-membrane interactions and lipids contained systems. Nevertheless, developing CG models and parameterizing them with a maintained simulation accuracy is a challenging task.

2.4.3.1. MARTINI force field

MARTINI is a CG force field that is named after the nickname of the city of Groningen where it was developed [72]. It uses a 4:1 mapping scheme which means four heavy atoms are represented by one center (CG bead) (See **Figure 2.1**). The bead mass is set to 72 amu which is equal to 4 water molecules. Moreover, small molecules such as benzene, cholesterol, and selected amino acids are mapped with enhanced resolution ≈ 2:1 and bead mass of 45 amu. There are four types of interactions that the model considers: polar, non-polar, apolar, and charged denoted by P, N, C, and Q respectively. In addition, the degree of polarity is ranged from low (1) to high (5), and the hydrogen bond capabilities are symbolized as donor (d), acceptor (a), both (da), or none (0).

Nonbonded interactions potential functions in MARTINI describe the relation between the pair of atoms i and j which separated by a distance of r_{ij} via Lennard-Jones (LJ) equation (See Equation **(2.1)**). ε_{ij} is the well-depth value that determines the interaction strength and ranged from 5.6 KJ/mol to 2.0 KJ/mol for strong polar groups interaction and polar-apolar interaction (hydrophobic effect) respectively. To govern the bead size, LJ parameter (σ) is set to 0.47 nm for normal bead types while for small molecules exception, σ = 0.43 nm, and the well-depth value is scaled to 75% of its standard.

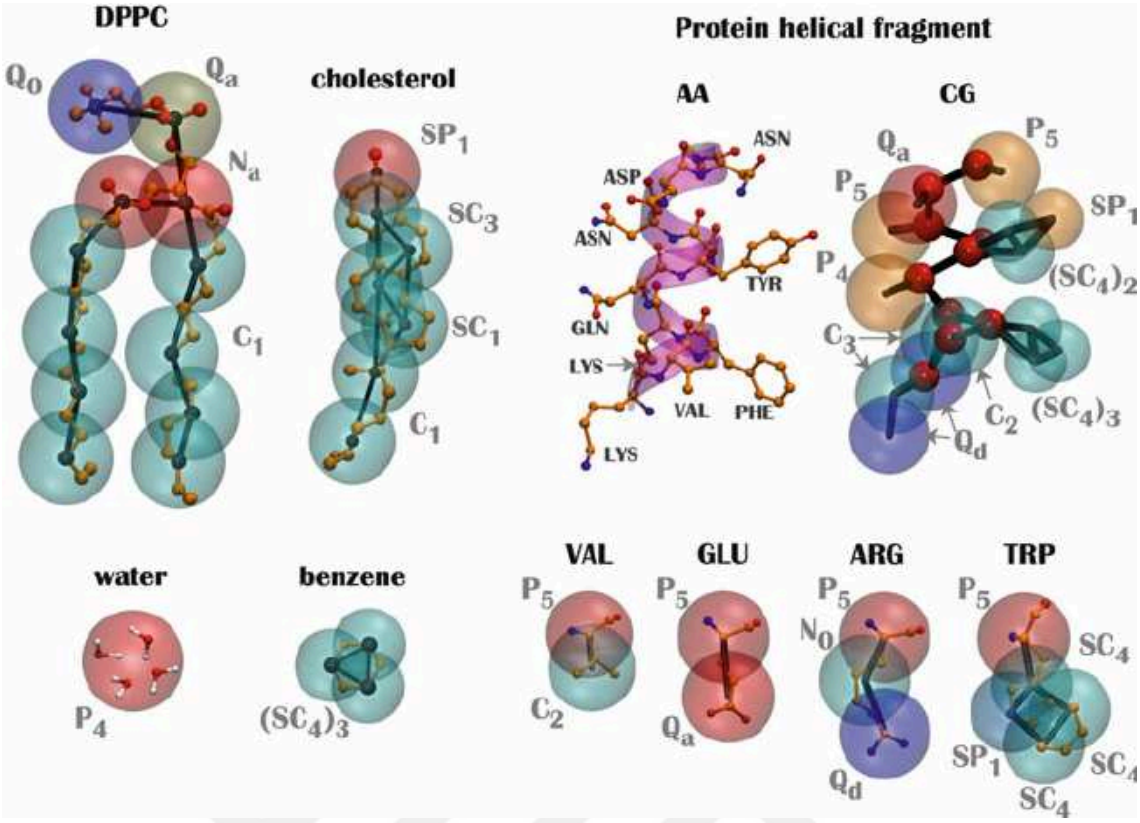

Figure 2.1: Illustration of the mapping scheme used in the MARTINI force field for DPPC, cholesterol, protein helical fragment, water, benzene, and four different amino acids. The CG beads are represented by transparent van der Waals spheres. In the protein helical fragment, the AA model is shown on the left and the CG model is on the right for simplification while combined for the other models. Hydrogens atoms are presented only in the water model. The figure is used with no modification from reference [73].

$$V_{LJ} = 4\varepsilon_{ij}[(\sigma_{ij})^{12} - (\sigma/r_{ij})^{6}] \quad \textbf{(2.1)}$$

Furthermore, the electrostatic interaction of the charged group (Q) is modeled using Coulomb's law (Equation **(2.2)**), where the relative dielectric constant (ε_{rel}) is set to 15 and charge is symbolized by q

$$V_{el} = q_i q_j / 4\pi\varepsilon_0\varepsilon_{rel} r_{ij} \quad \textbf{(2.2)}$$

It is worth noting that, the potential energy functions are shifted, LJ potential function is shifted from r_{shift} = 0.9 nm to r_{cut} = 1.2 nm, whereas the electrostatic potential function is shifted from r_{shift} = 0.0 nm to the same r_{cut} accordingly.

On the other hand, bonded interactions are modeled based on a set of potential functions

(Equations **(2.3) to (2.6)**):

$$V_b = 1/2K_b(d_{ij} - d_b)^2, \quad \textbf{(2.3)}$$

$$V_a = 1/2K_a[cos(\varphi_{ijk}) - cos(\varphi_a)]^2, \quad \textbf{(2.4)}$$

$$V_d = K_d[1 + cos(\theta_{ijkl} - \theta_d)], \quad \textbf{(2.5)}$$

$$V_{id} = K_{id}(\theta_{ijkl} - \theta_{id})^2, \quad \textbf{(2.6)}$$

which concern four interaction sites *i, j, k, l* separated by an equilibrium distance (d_b). The angle is denoted by (φ_a) and dihedral angles by (θ_d) and (θ_{id}). To induce flexibility of the molecule at CG level which results from the collective motions, force constants K are generally weak. The bonded potential (V_b) and angle potential (V_a) are used for the chemical bonded sites and representing the chain stiffness respectively. For the prevention of out-of-plane distortion of planar group, improper dihedral angle potential (V_{id}) is used, whereas the proper dihedral potential (V_d) is used for imposing secondary structure of the peptide backbone [72], [73].

2.4.3.2. Conversion of (CG) representation to (AA) representation (backmapping)

CG-MD simulations have lower resolution compared to AA-MD simulations. However, in certain scenarios, the conversion from CG to AA representation (Backmapping) is enhancing the analysis and provides more details at the atomic level. *Vickery et al.* developed a fragment-based tool "CG2AT2" for converting the CG models to AA ones [74]. It uses the rigid alignment of CG beads to a set of atomistic fragments that encode chemical and stereochemical information based on the selected force field. The tool is backmapping the CG system based on four fundamental steps: conversion, minimization, integration, and equilibration. Initially, the atomistic fragments are aligned to their corresponding CG beads based on the center of mass. Thereafter, the bond distances are minimized by rotating the aligned coordinates. The fragments are treated individually despite the knowledge

of their neighbors. Once the conversion is done, the system is minimized using steepest descent algorithm for the correction of bond lengths, angles, and steric clashes. Afterward, the system is reintegrated and minimized. For the detection of any threaded molecules which rarely present, abnormal bond lengths are used as indicators. finally, the system is equilibrated using NVT coupling scheme for 5 picoseconds (default time) restraining the Cα atoms in protein systems. Furthermore, for protein backmapping, the tool is provided two approaches: *de novo* and alignment. In the former, the atomistic structure is built up from the CG beads relying on its coordinates whereas, in the latter, a user-supplied AA structure is fitted to the CG coordinates. In addition to the structure alignment, sequence alignment is used for indexing the CG protein sequence according to the user-choice alignment group. In the case of missing residues in the submitted AA sequence compared to CG, both approaches are combined such that it can be modeled with *de novo* [74]–[80].

CHAPTER 3

3. EXPERIMENTAL PART

3.1. Homology Modeling and Systems Preparation

The three-dimensional (3D) crystal structure of *H.influenzae* FtsW/PBP3 is not available in the protein data bank (PDB). Therefore, Robetta server was used to model the structures [81]. FtsW (Uniprot ID: P45064) was modeled using RoseTTAFold [60] method with a confidence score of ≈ 0.8. Moreover, for PBP3 (Uniprot ID: P45059), the cytoplasmic part of the protein was excluded (residues 1 - 40) in modeling studies because it is out of the scope of the present study. The N-t was modeled using RoseTTAFold with a confidence score of ≈ 0.7, and the TP was modeled with comparative modeling. Different modeling methods were used based on the availability of homologous structures in the server confirmed databases. RodA-PBP2 complex crystal structure was available on the PDB [82] ID: 6PL5. All the structures were prepared using Maestro protein preparation tool implemented in Schrödinger [83], the missing residues were completed, and the mutations were introduced therein. The structures were submitted to the orientations of proteins in membranes (OPM) server [84] to properly align the macromolecules along the membrane axis. Thereafter, the pre-oriented target protein was submitted to "Martini maker's" module of CHARMM-GUI [85], [86] to build up the inner bacterial cell membrane, which contained 1-palmitoyl 2-cis-vaccenic phosphatidylethanolamine (PVPE) (90%), 1-palmitoyl 2-cis-vaccenic phosphatidylglycerol (PVPG) (5%), and Cardiolipin (CDL2) (5%) [87]. We used "ElNeDyn" martini model, which has been developed to control the conformation of the protein while keeping its internal dynamics [85], [88] and provided by the "Martini Maker" module of CHARMM-GUI, to model the protein in the system. In that way, large amplitude domain motions which were observed in atomistic simulations could be matched [89]. We used non-polarizable MARTINI water

model [90], where four water molecules are mapped to one water molecule and MARTINI 2.0 [72] force field to model membrane lipids.

3.2. Coarse-grained (CG) Molecular Dynamics (MD) Simulations Protocol

GROMACS [91] simulation package with *NPT* coupling scheme, which is tuned to generate constant number of particles, pressure, and temperature, was used to run the coarse-grained simulations for all systems (see **Table 3.1**). The simulations were run on a PC running Ubuntu 20.04.1 LTS on an Intel Core i7-7700 CPU. For the minimization and equilibration steps, velocity rescaling and Berendsen coupling algorithms were used with 1 ps and 5 ps coupling times to maintain a constant temperature of 310.15 K and a pressure of 1 bar, whereas the Parrinello-Rahman coupling algorithm was used in the production step with 15 ps coupling times and semi-isotropic coupling type. The time step for integration was set to 20 femtoseconds.

Table 3.1: Coarse-Grained (CG) molecular dynamics (MD) simulation lengths.

System // Replicate	**First**	**Second**	**Third**	**Fourth**
(WT PBP3)	2 μs	1 μs	1 μs	-
(Low-rPBP3)	1 μs	1 μs	1 μs	-
(High-rPBP3)	2 μs	1 μs	2 μs	-
(FtsW - WT PBP3)	1 μs	1 μs	1 μs	1 μs
(FtsW - High-rPBP3)	1 μs	1 μs	1 μs	1 μs
(FtsW - Low-rPBP3)	1 μs	1 μs	1 μs	-
(WT RodA - PBP2)	1 μs	1 μs	1 μs	-
(Hyperactive RodA - PBP2)	1 μs	1 μs	1 μs	-

3.3. Analysis

The trajectories were visualized with VMD [92] and the reaction coordinates of the angles/dihedrals were set accordingly. For further analysis, selected replicates of each system were converted back to the atomistic resolution with the help of an enhanced fragment based protocol named “CG2AT” [74]. The tool basically worked on a pre-defiend fragment based fitting criteria of the user-supplied coarse-grained structure. Moreover, the prediction of the allosteric contribution based on the submitted structure and its active site cavity was done with the help of the OHM server [93], [94]. OHM server repeats a series of stochastic process of perturbation propagation on a network of interacting

residues (submitted structure) using the built-in algorithm. The three-dimensional structure of cefixime and peptidoglycan substrate (D-alanyl-D-alanine) are available on PubChem [95] under the IDs of 5362065 and 5460362, respectively. The ligands are prepared and docked covalently to the target structures using "LigPrep" and "CovDock" modules of Schrödinger Maestro, respectively [96]. The plots of the study were prepared with the help of VMD [92], MATLAB (version 2018), and Origin (version 2022). Particularly, MATLAB was used to plot the probability distributions with the shaded area representing the standard error range while VMD and Origin were used for the 3D structures representations and histogram plots, respectively. All the plotted data represent statistical averages over the replicates of the systems studied (**Table 3.1**).

CHAPTER 4

4. RESULTS AND DISCUSSION

In the present work, we have defined more than one descriptor based on selected reaction coordinates to study the dynamics of the systems comparatively. **Table 4.1** provides a summary of the defined coordinates and the selected residues.

Table 4.1: Summary of the global coordinations defined in the present work.

Descriptor (Reference Figure)	**Residue No.(Domain)**	**Explanation**
Angle (**Figure 4.1**)	53(TM), 71(Nt), and 545(TP)	Mesures the distance between the TP and CM.
Dihedral Angle (**Figure 4.2**)	55(TM), 228(Nt), 448(TP), and 565(TP)	Defines the orientation of TP with respect to CM
Angle (**Figure 4.4**)	101(Nt), 174(Nt), and 241(Nt)	Describes the opening of the fork-structured N-t

4.1. The Mutations Impact Orientation of the TP Domain and Flexibility of the β3-β4 Loop

First, we set out to investigate possible local effects exerted by mutations on PBP3. *Sjodt et al.* proposed a model to explain the mechanism used by RodA/PBP2 complex of *T. thermophilus* for performing peptidoglycan synthesis [13] whereby PBP2 adopts two different conformations. These are compact and extended, which are required for accessing to the cellular membrane and newly formed peptidoglycan layer located on top of the cellular membrane, respectively. Therefore, we examined the generated trajectories to investigate if the mutations impacted orientation of the TP with respect to the membrane. To do so, we selected three points on the TM, N-t, and TP to describe an angle that reported on the proximity of TP with respect to membrane as shown in **Figure 4.1a**. WT, low- and high-rPBP3 sampled similar angles when they were in isolation as shown in **Figure 4.1b**. On

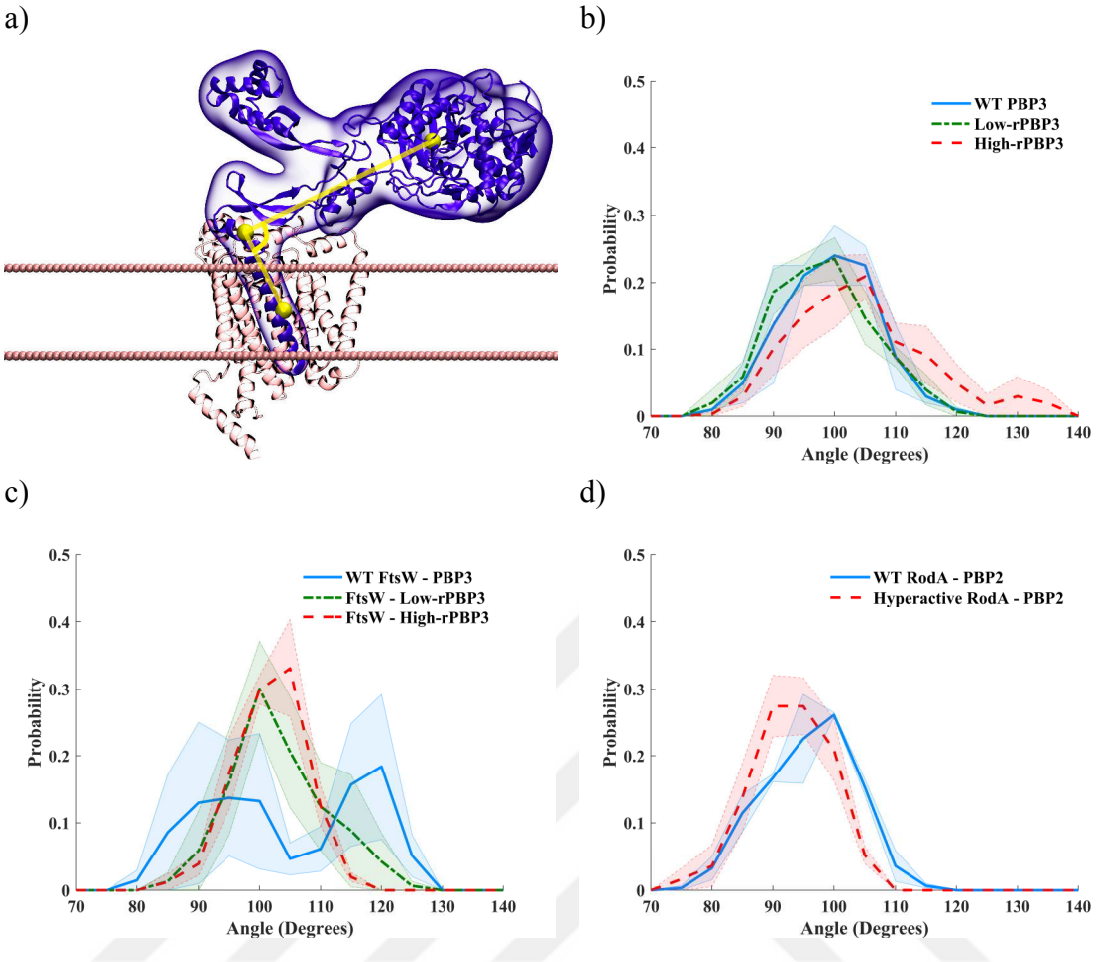

Figure 4.1: a) Schematic representation of the angle on 3D structure of PBP3. The CM is represented with two pink leaflets. The Cα atoms of the residues that were used to measure the angle were shown in yellow spheres with the direction. The probability distribution pertaining to the angle, which was measured among residues picked up on the TM, Nt, and TP domains, presented for **b)** WT and mutant PBP3 in isolation, **c)** complexes of WT and mutant PBP3 with FtsW, **d)** complexes of PBP2 with WT and Hyperactive RodA.

the other hand, WT could adopt both conformations when it was in complex with FtsW as evidenced by sampling of both lower and higher angles (**Figure 4.1c**). On the other hand, low- and high-rPBP3 sampled a narrower range of angles that were between 90-120 degrees when they were in complex with FtsW. It is also important to emphasize that the respective angle was measured in trajectories pertaining to hyperactive RodA/PBP2 complex and we observed that it adopted similar values to that of FtsW/low- and high-rPBP3 complex (**Figure 4.1d**).

In addition to the orientation of the TP, the mutation also impacted the positioning of the β-sheet (See **Figure 4.2a**) that surrounds the active site of PBP3. It adopted different orientations, namely conformation 1 and conformation 2, with respect to the membrane,

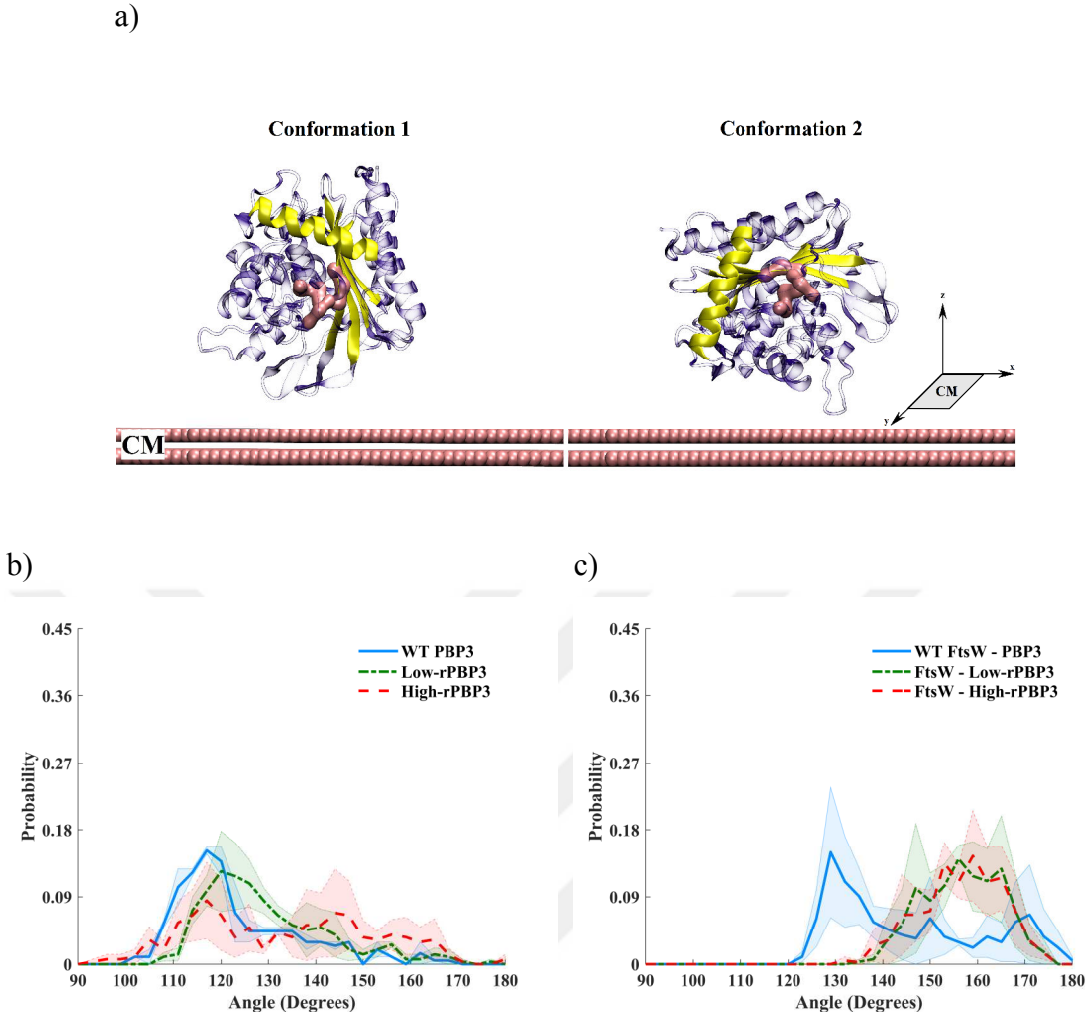

Figure 4.2: Probability distributions pertaining to dihedral angle that describes the orientation of the TP domain with respect to the membrane. Representative conformations are also shown. **a)** The placement of CM is symbolized by two-layered pink spheres. The core β-sheets are colored in yellow with one of the helix segments for the reader's orientation and the active site cavity is represented with surface representation in pink. Probability plots of the dihedral angle measured for WT and mutant **b)** PBP3s and **c)** FtsW-PBP3 complexes.

each of which was quantified by a dihedral angle that was measured using residues 55-228-448-565 located on TM, N-t, and α-helix 6 and α-helix 9, respectively. Accordingly, the β-sheet aligned parallel (140<angle<180) with respect to the membrane in conformation 2, whereas the rest of the angle values represented a perpendicular orientation of the β-sheet as depicted in **Figure 4.2a**. The WT PBP3 and low-rPBP3 adopted lower angle values whereas high-rPBP3 sampled both lower and higher values when it was in isolation displaying no preference towards any specific angle (**Figure 4.2b**). On the other hand, when WT and mutant PBP3s formed complex with FtsW, the systems adopted higher dihedral angles as shown in **Figure 4.2c**. It is important to emphasize that this orientational

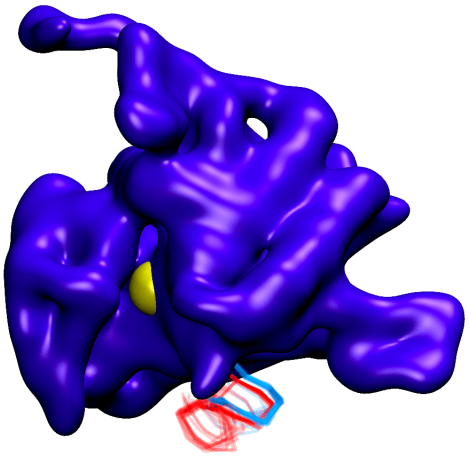

Figure 4.3: Schematic representation of β3-β4 loop with respect to time. Wild type and High-r are shown in cyan and red, respectively. The active site (Ser327) is shown in van der waals representation in yellow. The data for low-r is not shown for the sake of simplicity.

preference also impacted exposure of the active site of PBP3, where it was exposed toward the periplasmic site in the mutant PBP3s as shown in **Figure 4.2a**.

Moreover, we also examined if the flexibility of the β3-β4 loop was impacted since it was shown by *Singh et al.* that it modulated catalytic properties of the enzyme [52]. These authors showed that the flexibility of the loop decreased in cephalosporin-resistant *Neisseria gonorrhoeae*, which was needed for stabilizing the antibiotics in the active site, thus promoting acylation reaction in the wild type enzyme. Interestingly, we did not see any remarkable difference between wild type and mutant PBP3 when they were in isolation. On the other hand, we observed higher flexibility of the loop in both FtsW/low- and high-rPBP3 complex as shown in **Figure 4.3**. It is also important to emphasize that the loop was able to enter into the active site in trajectories pertaining to mutant FtsW/PBP3 complexes. Lastly, we also investigated the opening of the binding pocket by calculating an angle using C_α atoms of residues 358/498/550, which were located at the core of the β-sheet located on the TP domain and the loop that is known as a gatekeeper residue [14]. The pocket was slightly wider in WT than in mutant PBP3s (data not shown) and the difference became slightly larger when mutant PBP3s were complexed with FtsW.

4.2. The Opening of the Fork located on the N-t Differs Between Wild Type and Mutant PBP3s

The N-t has been shown to modulate the allosteric communication between PBP3 domains; however, the molecular mechanism has remained elusive [12]–[14], [97]. Towards this end, we examined the dynamics of the domain in trajectories pertaining to the wild type (WT) and mutant PBP3 as well as its complex with FtsW. The N-t structurally resembles a fork at the side far from the interface formed by the TP domain. We observed that the opening of the fork, which was described by the angle formed by residues 241/101/174, differed between WT and mutant proteins. Specifically, high-rPBP3 and low-rPBP3 were able to sample lower angle values compared to WT PBP3 (**Figure 4.4a**) when they were in isolation. The WT PBP3; however, showed tendency to sample higher values which were populated around 50° as shown in **Figure 4.4a**. In addition to lower angle values, mutant proteins could also sample higher values as WT PBP3 does, albeit with lower probability. We also examined the opening of the fork for the FtsW/PBP3 complex and showed that the angle was decreased in both WT and mutant proteins (**Figure 4.4c**) where mutant proteins could sample lower angle values compared to WT PBP3 as in the case of isolated PBP3. Furthermore, we also set out to investigate if the opening of the fork differs in other bPBP complexes. Towards this end, we examined the status of the fork by performing simulations using the crystal structure pertaining to RodA/PBP2 complex (PDB ID: 6PL5) using corresponding residue triplet, and showed that it could adopt higher angle values (See **Figure 4.4e**) than that by the FtsW/PBP3 complex. Moreover, we also examined the same opening in the mutant RodA/PBP2 complex, which was characterized as constitutively active, since it does not require elongasome activation signals to get activated [13], [28], [53], [98]. Similarly, we showed that the mutation that caused hyperactivation led to sampling of smaller angle values than WT RodA/PBP2 complex as shown in **Figure 4.4e**. Collectively, these results showed that mutations either causing hyperactivation or resistance tended to reduce the opening at the fork in the mutant PBP2/PBP3 compared to WT PBP2/PBP3.

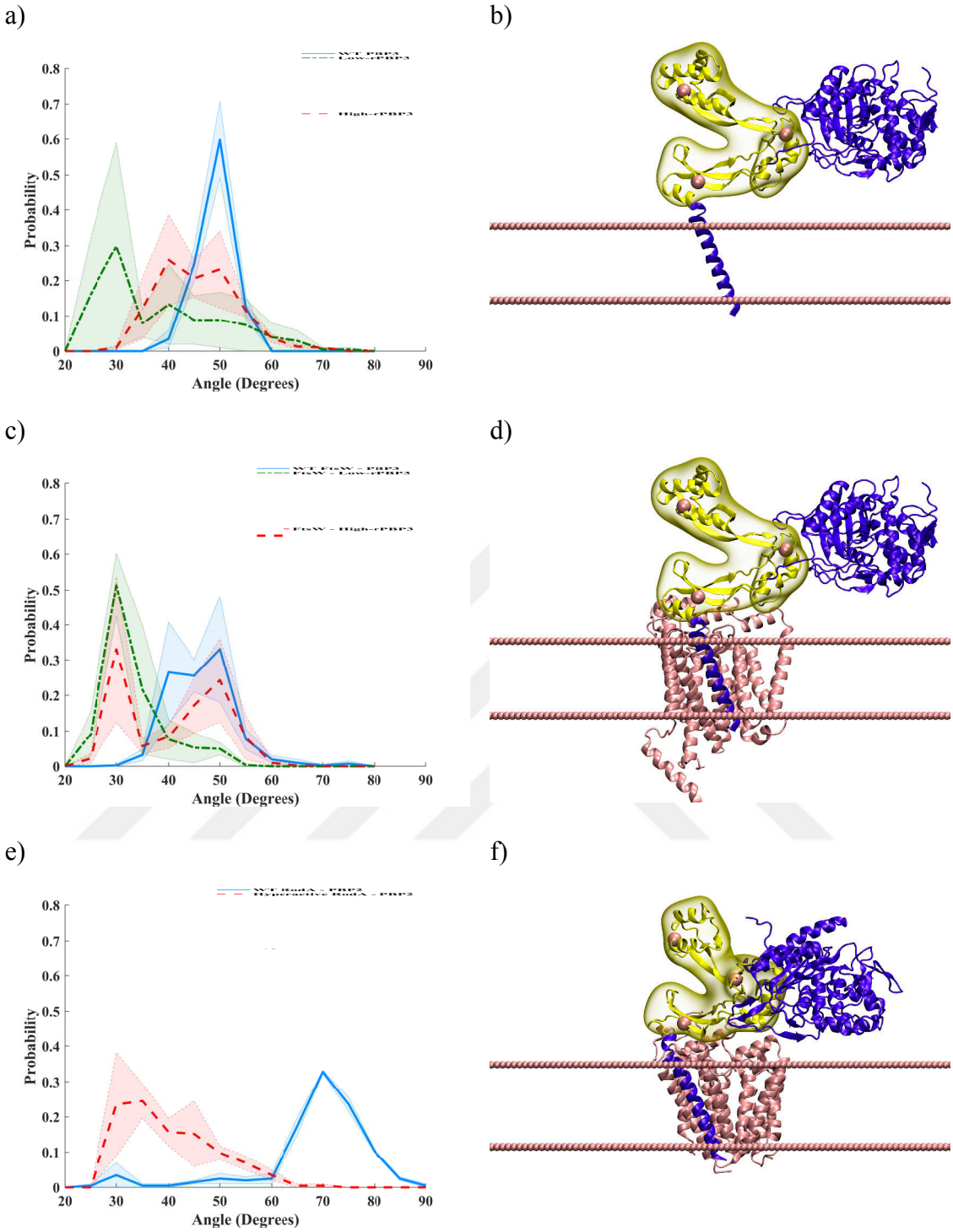

Figure 4.4: Probability distribution of the fork angle measured on the Nt domain of **a)** PBP3 in isolation with two resistance level along with the representative 3D model **b)**, **c)** FtsW-PBP3 complex along with the representative 3D model **d)**, **e)** RodA-PBP2 complex with the hyperactive phenotype along with representative 3D model **f)**. The CM is shown with the pink leaflets. The Cα atoms used to measure the angle are shown with pink spheres.

4.3. The Opening of the Fork Impacts the Proposed Allosteric Network between N-t and TP Domains

Having examined the dynamics of N-t in trajectories pertaining to WT and mutant PBP3s and their complexes by FtsW, we further set out to investigate if the preference observed for fork opening impacted hypothesized allosteric communication between the N-t and TP domains. Towards this end, we calculated the allosteric coupling intensity histograms of the systems using the OHM server (See **Section3.3** for details). The server requires an initial conformation and we provided representative conformations in which the most probable fork angle was adopted. Accordingly, we used the structure with low fork angle for the low-rPBP3 (around 30°) whereas two conformations with fork angles of 40 and 50° were used for high-rPBP3 since the probabilities pertaining to these angles were close to each other. On the other hand, we used one conformation for WT PBP3 that adopted a fork angle of 50°. The results showed that the number of residues contributing to the proposed allosteric interaction network connecting the N-t and TP was higher for both low- and high-rPBP3 compared to WT PBP3 as shown in **Figure 4.5**. It is also important to emphasize that we observed a similar pattern for WT and mutant FtsW/PBP3 complexes (data not shown). To further check if the number of allosteric residues was impacted by the fork angle, we picked up alternative conformations, other than the representative ones. For instance, we repeated the calculations using conformations with lower fork angles in WT trajectories. Interestingly, we observed that the number of the residues was fewer for conformations that were not representative of the systems. Moreover, we also mapped these residue clusters on the 3D structure of PBP3 and showed that participation of residues 258-274, 279-286, 292-298, making up α1, β1, and β2, respectively, was relatively higher in the systems studied (See gray regions in **Figure 4.5**). In fact, these residues make up the interaction interface between the N-t and TP domains. Similar region in PBP2a of methicillin-resistant *Staphylococcus aureus* was shown to be the target site for binding an allosteric non-covalent inhibitor [99]. Furthermore, number of such residues was higher in the mutant PBP3s compared to the WT protein as shown in **Figure 4.5**. Moreover, residues 446-458 on α7 showed higher contribution to the network in the mutant PBP3s than in the WT protein (See **Figure 4.5**). Finally, we observed that residues 310-330, which are located on the loops that connect the core segments of the TP domain, showed relatively higher contribution to the network compared to other residues.

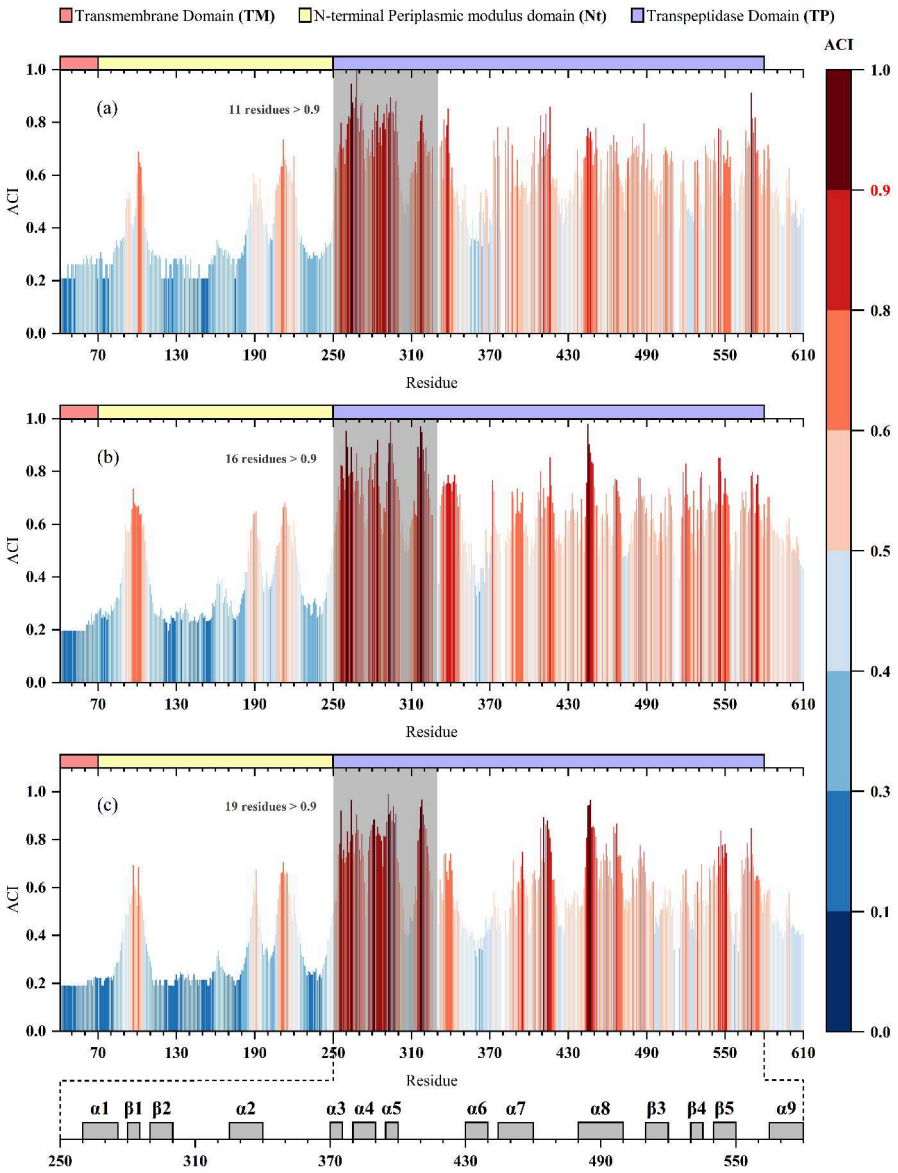

Figure 4.5: Allosteric Coupling Intensity Histograms calculated for **a)** WT PBP3, **b)** Low-rPBP3, and **c)** High-rPBP3 calculated via the OHM server.

Having observed that the mutation both impacted orientation of the β-sheet and the opening of the fork, we further investigated if certain fork angle values were associated with a specific orientation of the β-sheet, in particular in the mutant FtsW/PBP3 complex, since it adopted two different fork angle values (See **Figure 4.4c**). To do so, we clustered dihedral angle value/fork angle pairs using the trajectories pertaining to mutant complex and observed that the open form of the fork was preferred when perpendicular orientation of the β-sheet was adopted, whereas the closed form was preferred when the parallel orientation was adopted as shown in **Figure 4.6**. We further set out to examine if these fork angle/dihedral angle pairs impacted binding energies of both antibiotics and D-alanyl-D-alanine. Towards this end, we performed covalent-docking and peptide docking using

respective pairs that were picked up from trajectories pertaining to mutant and WT trajectories (See **Table 4.2**). We used cefixime as the antibiotic towards which the mutant PBP3 was shown to be resistant. We showed that the binding energy of the antibiotic was lower for the mutant than to the wild type, thus suggesting that the acylation reaction was more favorable for WT PBP3. It is important to emphasize that the two pairs, namely, low fork angle/parallel orientation and high fork angle/perpendicular conformation, displayed different patterns. The former could bind the antibiotics more favorably than the latter. Interestingly, the similar pattern was also observed in the binding energy of peptide substrate, namely D-alanyl-D-alanine.

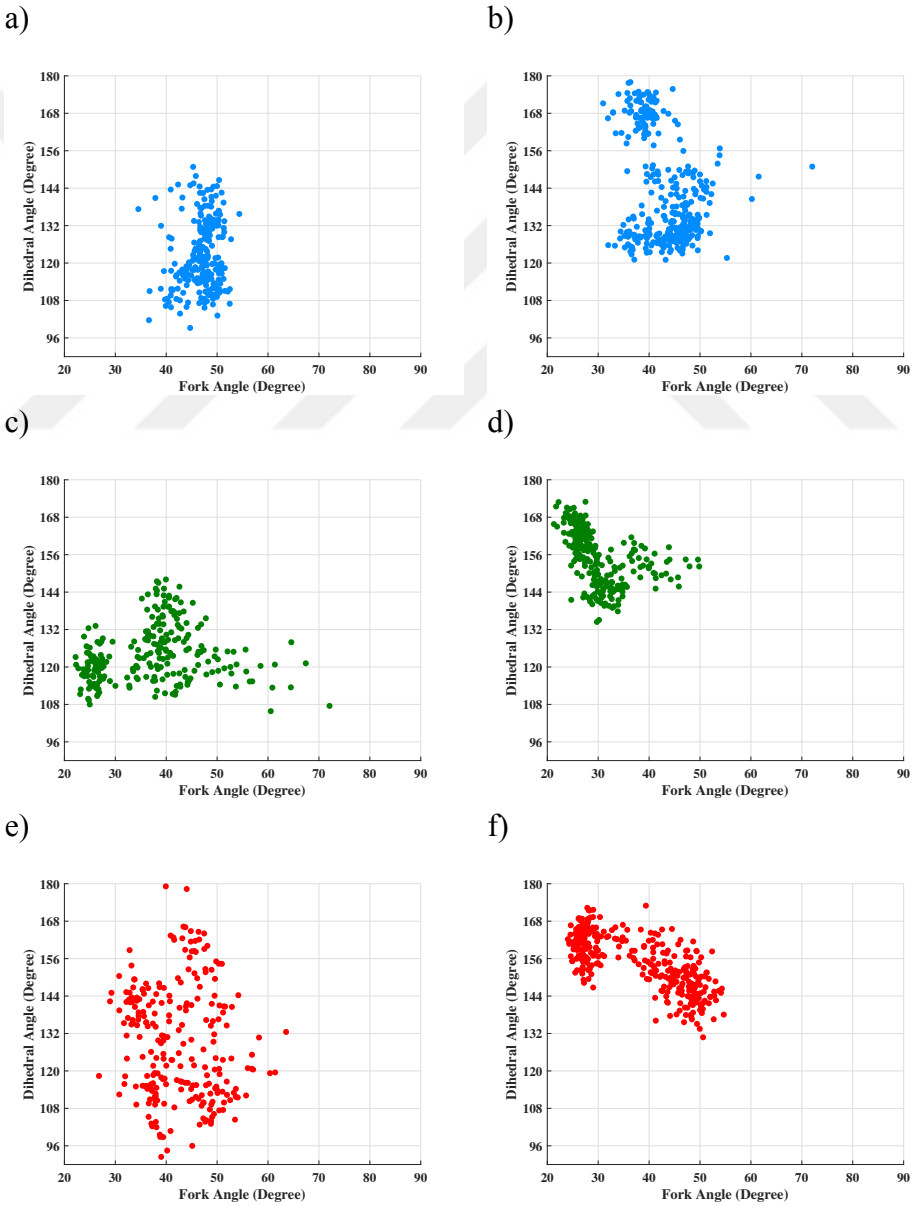

Figure 4.6: The 2D plots that show the correlation between the fork and the dihedral angle **a)** Wild type, **c)** single mutant, **e)** triple mutant PBP3s and their respective complexes formed by FtsW **b)**, **d)**, and **f)**.

Table 4.2: Covalent and peptide docking outputs. Conformation*: low fork angle and parallel orientation. Conformation**: high fork angle and perpendicular conformation.

System // Ligand	Cefixime	D-alanyl-D-alanine
WT PBP3	-4.21	-4.54
High-rPBP3*	-2.41	-4.15
High-rPBP3**	-1.03	-2.97

4.4. Discussion

In the present work, we provide an insight into large scale dynamics of β-lactam antibiotics resistant bacteria displaying different resistance levels due to bPBP-associated mutations. We showed that alterations in amino acids caused both local and non-local rearrangements in PBP3, which became more prominent in the case of the FtsW/PBP3 complex. For instance, the TP domain was positioned at a specific location with respect to FtsW and membrane in the mutant complex. Considering that maintenance of certain interactions formed between the extracellular region of FtsW and N-t domain of PBP3 is required for proper functioning of both PBP3 and FtsW, constraining the TP domain at a specific orientation might trigger peptidoglycan assembly during cell elongation, division, and sporulation. In relation with this, β3- β4 loop, which was previously shown to be responsible for maintaining the catalytic activity of the enzyme, was more flexible in the mutant FtsW/PBP3 complex. In addition to the TP, we also observed differences in the orientation of the catalytic site of PBP3. In particular, it was directed towards the periplasmic site, away from the cytoplasmic membrane in the mutant FtsW/PBP3 complex. Interestingly, we observed a similar behavior in the hyperactive mutant RodA/PBP2 complex, which did not require any external signal to activate cell wall synthesis. Moreover, we also demonstrated that affinity of the mutant PBP3 towards D-alanyl-D-alanine, which is the substrate that binds PBP3 in transpeptidation, was higher in conformations having exposed β-sheet to the periplasmic site.

Besides local rearrangements exerted by mutations, we also observed non-local modulation at the fork located on the N-t domain, at which divisome and elongasome partners, such as MreC [41], [100], bind. We showed that the closed fork was preferred in mutant FtsW/PBP3 complexes. Likewise, hyperactive RodA/PBP2 complex displayed similar behavior where the opening of the fork decreased upon complex formation. The closed fork was preferred when the active site of the mutant PBP3 was exposed towards the

periplasmic space. Lastly, we also showed that the opening of the fork modulated communication between TP and N-t domains of PBP3 where closed fork was shown to be associated with higher number of residues participating in the allosteric interaction network that was hypothesized to be present between the TP and N-t domains.

Cumulatively, the results of the study showed that the N-t of *H. influenzae* PBP3 emerges as a potential allosteric site which can be targeted for developing effective molecules that can modulate the function of mutant bacterial proteins which cause antibiotic resistance. In particular, the closed fork that is sampled by the mutant FtsW/PBP3 complex, can be stabilized by means of small therapeutics since it was shown to be associated with favorable binding of antibiotics and higher number of allosteric residues that provided communication between the N-t and TP domains. As such, this study provides a new perspective for identification of allosteric regions on the mutant bacterial proteins that cause antibiotic resistance.

CHAPTER 5

5. CONCLUSION AND FUTURE WORK

In 2019, resistant bacteria killed 1.27 million individuals around the world [101]. One in five of the deaths was a child under five years old. The morbidity rate is increasing and there is an urgent call to combat this silent pandemic. Bacteria aimed to survive in all environmental conditions, consequently, trying to resist any factor that threatens their life. Resistant bacteria (superbugs) can survive even in the presence of antibacterial drugs. Despite the need of developing new agents, understanding the resistance mechanisms might help in restoring the efficiency of the currently available antibiotics against resistant bacteria.

β-lactam antibiotics, the most used antibiotics worldwide, are targeting the enzymes that catalyze cell wall synthesis namely PBPs. However, bacteria acquire mutations in/around the active sites of those enzymes to develop resistance. The resistance, although poorly identified, is supposed to impact enzymatic reaction rate and/or ligand-receptor binding affinity. Consequently, at a molecular level, emphasizing the effect of resistance mutations on the dynamics of mutant macromolecules would provide insight into combating resistant bacteria.

In the present work, we have explored the impact of resistance causing triple-set mutation (S385T + L389F + N526K) and its subset (N526K) on PBP3 of *H. influenzae* in isolation and complexed with FtsW. The effects are studied against the backdrop of WT systems and another SEDS-bPBP system (RodA-PBP2 of *T. thermophilus*) in either type WT and Hyperactive mutant. We showed that the triple/single point mutation had local and nonlocal consequences on PBP3 and FtsW/PBP3. Moreover, in complex, the systems appeared to have directed behavior when sampling conformational changes in space compared to isolated systems. The resistance mutations impacted the localization/orientation

of TP with respect to CM. In addition, the opening of the catalytic site and the dynamics of a surrounding loop region are distinguishable between WT and mutant systems. The proposed allosteric network shows a higher number of contributors in resistant systems, hence, preferable communication within PBP3 domains. Furthermore, we investigated the dynamics of N-t and proposed it can be an allosteric modulator that is able to maintain sampling dominant conformations which stabilizes the system and ought to affect the resistance level. It was able to do so by switching between opened and closed fork angle states. Importantly, covalent docking and peptide docking studies support the proposed hypothesis.

In the future, the regions which are highly contributing to the allosteric network might be targeted after defining hypothesized allosteric pocket. However, in this work, we have focused on PBP3-associated mutation, while the scope might be extended to include mutation points introduced to FtsW. In literature, the defined mutations of FtsW are responsible for impacting the complex phenotype (active/inactive) by accessing the signaling cascade of the divisome, but the mechanism is elusive. In contrast, we can maximize the research scope to study the structural/dynamic consequences of FtsW-associated mutations on SEDS-bPBP complexes.

BIBLIOGRAPHY

[1] M. Hutchings, A. Truman, and B. Wilkinson, 'Antibiotics: past, present and future', *Curr. Opin. Microbiol.*, vol. 51, pp. 72–80, Oct. 2019, doi: 10.1016/J.MIB.2019.10.008.

[2] A. O'Rourke *et al.*, 'Mechanism-of-action classification of antibiotics by global transcriptome profiling', *Antimicrob. Agents Chemother.*, vol. 64, no. 3, 2020, doi: 10.1128/AAC.01207-19/SUPPL_FILE/AAC.01207-19-SD009.XLSX.

[3] W. Qin, M. Panunzio, and S. Biondi, 'β-Lactam Antibiotics Renaissance', *Antibiot. 2014, Vol. 3, Pages 193-215*, vol. 3, no. 2, pp. 193–215, May 2014, doi: 10.3390/ANTIBIOTICS3020193.

[4] L. M. Lima, B. N. M. da Silva, G. Barbosa, and E. J. Barreiro, 'β-lactam antibiotics: An overview from a medicinal chemistry perspective', *Eur. J. Med. Chem.*, vol. 208, p. 112829, Dec. 2020, doi: 10.1016/J.EJMECH.2020.112829.

[5] Y. Sanbongi, T. Suzuki, Y. Osaki, N. Senju, T. Ida, and K. Ubukata, 'Molecular Evolution of β-Lactam-Resistant Haemophilus influenzae: 9-Year Surveillance of Penicillin-Binding Protein 3 Mutations in Isolates from Japan', *Antimicrob. Agents Chemother.*, vol. 50, no. 7, pp. 2487–2492, Jul. 2006, doi: 10.1128/AAC.01316-05.

[6] Y. Osaki *et al.*, 'Genetic Approach To Study the Relationship between Penicillin-Binding Protein 3 Mutations and Haemophilus influenzae β-Lactam Resistance by Using Site-Directed Mutagenesis and Gene Recombinants', *Antimicrob. Agents Chemother.*, vol. 49, no. 7, pp. 2834–2839, Jul. 2005, doi: 10.1128/AAC.49.7.2834-2839.2005.

[7] K. V. Mahasenan *et al.*, 'Conformational dynamics in penicillin-binding protein 2a of methicillin-resistant staphylococcus aureus, allosteric communication network and enablement of catalysis', *J. Am. Chem. Soc.*, vol. 139, no. 5, pp. 2102–2110, Feb. 2017, doi: 10.1021/JACS.6B12565/SUPPL_FILE/JA6B12565_SI_002.AVI.

[8] E. Sauvage, F. Kerff, M. Terrak, J. A. Ayala, and P. Charlier, 'The penicillin-binding proteins: structure and role in peptidoglycan biosynthesis', *FEMS Microbiol. Rev.*, vol. 32, no. 2, pp. 234–258, Mar. 2008, doi: 10.1111/J.1574-6976.2008.00105.X.

[9] W. Vollmer, D. Blanot, and M. A. De Pedro, 'Peptidoglycan structure and architecture', *FEMS Microbiol. Rev.*, vol. 32, no. 2, pp. 149–167, Mar. 2008, doi: 10.1111/J.1574-6976.2007.00094.X.

[10] C. Goffin and J.-M. Ghuysen, 'Multimodular Penicillin-Binding Proteins: An Enigmatic Family of Orthologs and Paralogs', *Microbiol. Mol. Biol. Rev.*, vol. 62, no. 4, pp. 1079–1093, Dec. 1998, doi: 10.1128/MMBR.62.4.1079-1093.1998/ASSET/B08D9270-A039-4ED5-8160-55150C72F404/ASSETS/GRAPHIC/MR0480036009.JPEG.

[11] P. Macheboeuf, C. Contreras-Martel, V. Job, O. Dideberg, and A. Dessen, 'Penicillin Binding Proteins: key players in bacterial cell cycle and drug resistance processes', *FEMS Microbiol. Rev.*, vol. 30, no. 5, pp. 673–691, Sep. 2006, doi: 10.1111/J.1574-6976.2006.00024.X.

[12] D. Bellini, L. Koekemoer, H. Newman, and C. G. Dowson, 'Novel and Improved Crystal Structures of H. influenzae, E. coli and P. aeruginosa Penicillin-Binding Protein 3 (PBP3) and N. gonorrhoeae PBP2: Toward a Better Understanding of β-Lactam Target-Mediated Resistance', *J. Mol. Biol.*, vol. 431, no. 18, pp. 3501–3519, Aug. 2019, doi: 10.1016/J.JMB.2019.07.010.

[13] M. Sjodt *et al.*, 'Structural coordination of polymerization and crosslinking by a SEDS–bPBP peptidoglycan synthase complex', *Nat. Microbiol.*, 2020, doi: 10.1038/s41564-020-0687-z.

[14] L. H. Otero *et al.*, 'How allosteric control of Staphylococcus aureus penicillin binding protein 2a enables methicillin resistance and physiological function', *Proc. Natl. Acad. Sci. U. S. A.*, vol. 110, no. 42, pp. 16808–16813, Oct. 2013, doi: 10.1073/PNAS.1300118110/SUPPL_FILE/PNAS.201300118SI.PDF.

[15] D. Skaare *et al.*, 'Emergence of clonally related multidrug resistant Haemophilus influenzae with penicillin-binding protein 3-mediated resistance to extended-spectrum cephalosporins, Norway, 2006 to 2013', *Eurosurveillance*, vol. 19, no. 49, p. 20986, Dec. 2014, doi: 10.2807/1560-7917.ES2014.19.49.20986/CITE/PLAINTEXT.

[16] D. Skaare *et al.*, 'Multilocus sequence typing and ftsI sequencing: A powerful tool for surveillance of penicillin-binding protein 3-mediated beta-lactam resistance in nontypeable Haemophilus influenzae', *BMC Microbiol.*, vol. 14, no. 1, pp. 1–16, May 2014, doi: 10.1186/1471-2180-14-131/TABLES/6.

[17] S. Bin Zaman *et al.*, 'A Review on Antibiotic Resistance: Alarm Bells are Ringing', *Cureus J. Med. Sci.*, vol. 9, no. 6, Jun. 2017, doi: 10.7759/CUREUS.1403.

[18] A. MacGowan and E. Macnaughton, 'Antibiotic resistance', *Medicine (Baltimore).*, vol. 45, no. 10, pp. 622–628, Oct. 2017, doi: 10.1016/J.MPMED.2017.07.006.

[19] A. Chokshi, Z. Sifri, D. Cennimo, and H. Horng, 'Global Contributors to Antibiotic Resistance', *J. Glob. Infect. Dis.*, vol. 11, no. 1, p. 36, Jan. 2019, doi: 10.4103/JGID.JGID_110_18.

[20] M. A. Mahmoud, M. Aldhaeefi, A. Sheikh, and H. Aljadhey, 'Community pharmacists' perspectives about reasons behind antibiotics dispensing without prescription: a qualitative study', *Biomed. Res.*, vol. 29, no. 21, pp. 3792–3796, Nov. 2018, doi: 10.4066/BIOMEDICALRESEARCH.29-18-1112.

[21] M. K. Sreeja, N. L. Gowrishankar, S. Adisha, and K. C. Divya, 'Antibiotic resistance-reasons and the most common resistant pathogens – A review', *Res. J. Pharm. Technol.*, vol. 10, no. 6, pp. 1886–1890, 2017, doi: 10.5958/0974-360X.2017.00331.6.

[22] M. J. Culyba, C. Y. Mo, and R. M. Kohli, 'Targets for Combating the Evolution of Acquired Antibiotic Resistance', *Biochemistry*, vol. 54, no. 23, pp. 3573–3582, Jun. 2015, doi: 10.1021/ACS.BIOCHEM.5B00109/ASSET/IMAGES/LARGE/BI-2015-001092_0007.JPEG.

[23] N. A. Lerminiaux and A. D. S. Cameron, 'Horizontal transfer of antibiotic

resistance genes in clinical environments', *Can. J. Microbiol.*, vol. 65, no. 1, pp. 34–44, 2019, doi: 10.1139/CJM-2018-0275/ASSET/IMAGES/CJM-2018-0275TAB1.GIF.

[24] J. Lin, K. Nishino, M. C. Roberts, M. Tolmasky, R. I. Aminov, and L. Zhang, 'Mechanisms of antibiotic resistance', *Front. Microbiol.*, vol. 6, no. FEB, p. 34, Feb. 2015, doi: 10.3389/FMICB.2015.00034/BIBTEX.

[25] M. S. Wilke, A. L. Lovering, and N. C. J. Strynadka, 'β-Lactam antibiotic resistance: a current structural perspective', *Curr. Opin. Microbiol.*, vol. 8, no. 5, pp. 525–533, Oct. 2005, doi: 10.1016/J.MIB.2005.08.016.

[26] K. Poole, 'Resistance to β-lactam antibiotics', *Cell. Mol. Life Sci.*, vol. 61, no. 17, pp. 2200–2223, Sep. 2004, doi: 10.1007/S00018-004-4060-9/METRICS.

[27] L. Lingzhi *et al.*, 'The role of two-component regulatory system in β-lactam antibiotics resistance', *Microbiol. Res.*, vol. 215, pp. 126–129, Oct. 2018, doi: 10.1016/J.MICRES.2018.07.005.

[28] A. J. F. Egan, J. Errington, and W. Vollmer, 'Regulation of peptidoglycan synthesis and remodelling', *Nat. Rev. Microbiol. 2020 188*, vol. 18, no. 8, pp. 446–460, May 2020, doi: 10.1038/s41579-020-0366-3.

[29] M. G. P. Page, 'Beta-lactam antibiotics', *Antibiot. Discov. Dev.*, vol. 9781461414001, pp. 79–117, Apr. 2012, doi: 10.1007/978-1-4614-1400-1_3/COVER.

[30] P. A. Ropp, M. Hu, M. Olesky, and R. A. Nicholas, 'Mutations in ponA, the gene encoding penicillin-binding protein 1, and a novel locus, penC, are required for high-level chromosomally mediated penicillin resistance in Neisseria gonorrhoeae', *Antimicrob. Agents Chemother.*, vol. 46, no. 3, pp. 769–777, 2002, doi: 10.1128/AAC.46.3.769-777.2002/ASSET/37751250-78C9-4CB2-BDD7-D573C90F5893/ASSETS/GRAPHIC/AC032062702B.JPEG.

[31] S. D. Makover, R. Wright, and E. Telep, 'Penicillin-binding proteins in Haemophilus influenzae', *Antimicrob. Agents Chemother.*, vol. 19, no. 4, pp. 584–588, 1981, doi: 10.1128/AAC.19.4.584.

[32] A. J. Meeske *et al.*, 'SEDS proteins are a widespread family of bacterial cell wall polymerases', *Nat. 2016 5377622*, vol. 537, no. 7622, pp. 634–638, Aug. 2016, doi: 10.1038/nature19331.

[33] A. J. F. Egan and W. Vollmer, 'The physiology of bacterial cell division', *Ann. N. Y. Acad. Sci.*, vol. 1277, no. 1, pp. 8–28, Jan. 2013, doi: 10.1111/J.1749-6632.2012.06818.X.

[34] C. Otten, M. Brilli, W. Vollmer, P. H. Viollier, and J. Salje, 'Peptidoglycan in obligate intracellular bacteria', *Mol. Microbiol.*, vol. 107, no. 2, pp. 142–163, Jan. 2018, doi: 10.1111/MMI.13880.

[35] A. Taguchi *et al.*, 'FtsW is a peptidoglycan polymerase that is functional only in complex with its cognate penicillin-binding protein', *Nat. Microbiol. 2019 44*, vol. 4, no. 4, pp. 587–594, Jan. 2019, doi: 10.1038/s41564-018-0345-x.

[36] B. Lara and J. A. Ayala, 'Topological characterization of the essential Escherichia coli cell division protein FtsW', *FEMS Microbiol. Lett.*, vol. 216,

no. 1, pp. 23–32, Oct. 2002, doi: 10.1111/J.1574-6968.2002.TB11409.X.

[37] T. Mohammadi *et al.*, 'Identification of FtsW as a transporter of lipid-linked cell wall precursors across the membrane', *EMBO J.*, vol. 30, no. 8, pp. 1425–1432, Apr. 2011, doi: 10.1038/EMBOJ.2011.61.

[38] T. Mohammadi *et al.*, 'Specificity of the transport of lipid II by FtsW in Escherichia coli', *J. Biol. Chem.*, vol. 289, no. 21, pp. 14707–14718, May 2014, doi: 10.1074/jbc.M114.557371.

[39] M. Sjodt *et al.*, 'Structure of the peptidoglycan polymerase RodA resolved by evolutionary coupling analysis', *Nat. 2018 5567699*, vol. 556, no. 7699, pp. 118–121, Mar. 2018, doi: 10.1038/nature25985.

[40] K. T. Park, S. Du, and J. Lutkenhaus, 'Essential role for ftsl in activation of septal peptidoglycan synthesis', *MBio*, vol. 11, no. 6, pp. 1–17, Nov. 2020, doi: 10.1128/MBIO.03012-20/SUPPL_FILE/MBIO.03012-20-ST001.DOCX.

[41] A. Martins *et al.*, 'Self-association of MreC as a regulatory signal in bacterial cell wall elongation', *Nat. Commun. 2021 121*, vol. 12, no. 1, pp. 1–10, May 2021, doi: 10.1038/s41467-021-22957-9.

[42] S. Tristram, M. R. Jacobs, and P. C. Appelbaum, 'Antimicrobial resistance in Haemophilus influenzae', *Clin. Microbiol. Rev.*, vol. 20, no. 2, pp. 368–389, Apr. 2007, doi: 10.1128/CMR.00040-06/ASSET/B1C94A0B-84FA-4350-B2BC-9AFC551DAC68/ASSETS/GRAPHIC/ZCM0020722040003.JPEG.

[43] S. Brunton, 'Current face of acute otitis media: Microbiology and prevalence resulting from widespread use of heptavalent pneumococcal conjugate vaccine', *Clin. Ther.*, vol. 28, no. 1, pp. 118–123, Jan. 2006, doi: 10.1016/J.CLINTHERA.2006.01.011.

[44] A. Apisarnthanarak and L. M. Mundy, 'Etiology of community-acquired pneumonia', *Clin. Chest Med.*, vol. 26, no. 1, pp. 47–55, Mar. 2005, doi: 10.1016/j.ccm.2004.10.016.

[45] 'Haemophilus influenzae type b (Hib)'. https://www.who.int/europe/news-room/fact-sheets/item/haemophilus-influenzae-type-b-(hib) (accessed Feb. 02, 2023).

[46] J. Thegerström, E. Matuschek, Y. C. Su, K. Riesbeck, and F. Resman, 'A novel PBP3 substitution in Haemophilus influenzae confers reduced aminopenicillin susceptibility', *BMC Microbiol.*, vol. 18, no. 1, pp. 1–7, May 2018, doi: 10.1186/S12866-018-1196-6/TABLES/3.

[47] V. Jakubu, L. Malisova, M. Musilek, K. Pomorska, and H. Zemlickova, 'Characterization of haemophilus influenzae strains with non-enzymatic resistance to β-lactam antibiotics caused by mutations in the pbp3 gene in the czech republic in 2010–2018', *Life*, vol. 11, no. 11, p. 1260, Nov. 2021, doi: 10.3390/LIFE11111260/S1.

[48] K. Hasegawa *et al.*, 'Rapidly Increasing Prevalence of β-Lactamase-Nonproducing, Ampicillin-Resistant Haemophilus influenzae Type b in Patients with Meningitis', *Antimicrob. Agents Chemother.*, vol. 48, no. 5, pp. 1509–1514, May 2004, doi: 10.1128/AAC.48.5.1509-1514.2004/ASSET/783FB702-E05E-

4D18-A810-D79092127339/ASSETS/GRAPHIC/ZAC0050440090001.JPEG.

[49] J. Tomberg, M. Unemo, C. Davies, and R. A. Nicholas, 'Molecular and structural analysis of mosaic variants of penicillin-binding protein 2 conferring decreased susceptibility to expanded-spectrum cephalosporins in Neisseria gonorrhoeae: Role of epistatic mutations', *Biochemistry*, vol. 49, no. 37, pp. 8062–8070, Sep. 2010, doi: 10.1021/BI101167X/SUPPL_FILE/BI101167X_SI_001.TIF.

[50] A. Singh *et al.*, 'Mutations in penicillin-binding protein 2 from cephalosporin-resistant Neisseria gonorrhoeae hinder ceftriaxone acylation by restricting protein dynamics', *J. Biol. Chem.*, vol. 295, no. 21, pp. 7529–7543, May 2020, doi: 10.1074/JBC.RA120.012617/ATTACHMENT/FAA08319-D43D-413B-ADFC-B0784505BC59/MMC1.PDF.

[51] B. A. Fenton, J. Tomberg, C. A. Sciandra, R. A. Nicholas, C. Davies, and P. Zhou, 'Mutations in PBP2 from ceftriaxone-resistant Neisseria gonorrhoeae alter the dynamics of the β3–β4 loop to favor a low-affinity drug-binding state', *J. Biol. Chem.*, vol. 279, no. 4, Oct. 2021, doi: 10.1016/j.jbc.2021.101188.

[52] A. Singh, J. Tomberg, R. A. Nicholas, and C. Davies, 'Recognition of the β-lactam carboxylate triggers acylation of Neisseria gonorrhoeae penicillin-binding protein 2', *J. Biol. Chem.*, vol. 294, no. 38, pp. 14020–14032, Sep. 2019, doi: 10.1074/JBC.RA119.009942/ATTACHMENT/9166E3B2-3A2B-4A76-948A-03EB5294DB74/MMC1.PDF.

[53] Y. Li *et al.*, 'Genetic analysis of the septal peptidoglycan synthase FtsWI complex supports a conserved activation mechanism for SEDS-bPBP complexes', *PLOS Genet.*, vol. 17, no. 4, p. e1009366, Apr. 2021, doi: 10.1371/JOURNAL.PGEN.1009366.

[54] E. Krieger, S. B. Nabuurs, and G. Vriend, 'HOMOLOGY MODELING'.

[55] G. Chinea, G. Padron, R. W. W. Hooft, C. Sander, and G. Vriend, 'The use of position-specific rotamers in model building by homology', *Proteins Struct. Funct. Bioinforma.*, vol. 23, no. 3, pp. 415–421, Nov. 1995, doi: 10.1002/PROT.340230315.

[56] C. Dodge, R. Schneider, and C. Sander, 'The HSSP database of protein structure—sequence alignments and family profiles', *Nucleic Acids Res.*, vol. 26, no. 1, pp. 313–315, Jan. 1998, doi: 10.1093/NAR/26.1.313.

[57] A. Fiser, R. Kinh, G. Do, and A. S. ˇ Ali, 'Modeling of loops in protein structures', *Protein Sci.*, vol. 9, no. 9, pp. 1753–1773, Jan. 2000, doi: 10.1110/PS.9.9.1753.

[58] K. T. Simons, R. Bonneau, I. Ruczinski, and D. Baker, 'AB INITIO: PREDICTION REPORTS Ab Initio Protein Structure Prediction of CASP III Targets Using ROSETTA', doi: 10.1002/(SICI)1097-0134(1999)37:3.

[59] M. J. Sippl, 'Calculation of conformational ensembles from potentials of mena force: An approach to the knowledge-based prediction of local structures in globular proteins', *J. Mol. Biol.*, vol. 213, no. 4, pp. 859–883, Jun. 1990, doi: 10.1016/S0022-2836(05)80269-4.

[60] M. Baek *et al.*, 'Accurate prediction of protein structures and interactions using a three-track neural network', *Science (80-.).*, vol. 373, no. 6557, pp. 871–876, Aug. 2021, doi: 10.1126/SCIENCE.ABJ8754/SUPPL_FILE/ABJ8754_MDAR_REPRODUCIBILITY_CHECKLIST.PDF.

[61] J. Jumper *et al.*, 'Highly accurate protein structure prediction with AlphaFold', *Nat. 2021 5967873*, vol. 596, no. 7873, pp. 583–589, Jul. 2021, doi: 10.1038/s41586-021-03819-2.

[62] A. W. Senior *et al.*, 'Improved protein structure prediction using potentials from deep learning', *Nat. 2020 5777792*, vol. 577, no. 7792, pp. 706–710, Jan. 2020, doi: 10.1038/s41586-019-1923-7.

[63] J. D. Durrant and J. A. McCammon, 'Molecular dynamics simulations and drug discovery', *BMC Biol.*, vol. 9, no. 1, pp. 1–9, Oct. 2011, doi: 10.1186/1741-7007-9-71/FIGURES/4.

[64] E. Brunk and U. Rothlisberger, 'Mixed Quantum Mechanical/Molecular Mechanical Molecular Dynamics Simulations of Biological Systems in Ground and Electronically Excited States', *Chem. Rev.*, vol. 115, no. 12, pp. 6217–6263, Jun. 2015, doi: 10.1021/CR500628B/ASSET/IMAGES/CR500628B.SOCIAL.JPEG_V03.

[65] J. A. McCammon, B. R. Gelin, and M. Karplus, 'Dynamics of folded proteins', *Nat. 1977 2675612*, vol. 267, no. 5612, pp. 585–590, 1977, doi: 10.1038/267585a0.

[66] C. I. Bayly *et al.*, 'A Second Generation Force Field for the Simulation of Proteins, Nucleic Acids, and Organic Molecules', *J. Am. Chem. Soc.*, vol. 117, no. 19, pp. 5179–5197, 1995, doi: 10.1021/JA00124A002/ASSET/JA00124A002.FP.PNG_V03.

[67] L.-J. J. E., 'On the determination of molecular fields. II. From the equation of state of gas', *Proc. Roy. Soc. A*, vol. 106, pp. 463–477, 1924.

[68] J. Wang, R. M. Wolf, J. W. Caldwell, P. A. Kollman, and D. A. Case, 'Development and testing of a general amber force field', *J. Comput. Chem.*, vol. 25, no. 9, pp. 1157–1174, Jul. 2004, doi: 10.1002/JCC.20035.

[69] B. R. Brooks, R. E. Bruccoleri, B. D. Olafson, D. J. States, S. Swaminathan, and M. Karplus, 'CHARMM: A program for macromolecular energy, minimization, and dynamics calculations', *J. Comput. Chem.*, vol. 4, no. 2, pp. 187–217, Jun. 1983, doi: 10.1002/JCC.540040211.

[70] M. Christen *et al.*, 'The GROMOS software for biomolecular simulation: GROMOS05', *J. Comput. Chem.*, vol. 26, no. 16, pp. 1719–1751, Dec. 2005, doi: 10.1002/JCC.20303.

[71] D. A. Case *et al.*, 'The Amber biomolecular simulation programs', *J. Comput. Chem.*, vol. 26, no. 16, pp. 1668–1688, Dec. 2005, doi: 10.1002/JCC.20290.

[72] S. J. Marrink, H. J. Risselada, S. Yefimov, D. P. Tieleman, and A. H. De Vries, 'The MARTINI Force Field: Coarse Grained Model for Biomolecular Simulations', *J. Phys. Chem. B*, vol. 111, no. 27, pp. 7812–7824, Jul. 2007, doi:

10.1021/JP071097F.

[73] X. Periole and S.-J. Marrink, ‘The Martini Coarse-Grained Force Field’, pp. 533–565, 2013, doi: 10.1007/978-1-62703-017-5_20/COVER.

[74] O. N. Vickery and P. J. Stansfeld, ‘CG2AT2: An Enhanced Fragment-Based Approach for Serial Multi-scale Molecular Dynamics Simulations’, *J. Chem. Theory Comput.*, vol. 17, no. 10, pp. 6472–6482, Oct. 2021, doi: 10.1021/ACS.JCTC.1C00295/ASSET/IMAGES/LARGE/CT1C00295_0008.JPEG.

[75] T. A. Wassenaar, K. Pluhackova, R. A. Böckmann, S. J. Marrink, and D. P. Tieleman, ‘Going backward: A flexible geometric approach to reverse transformation from coarse grained to atomistic models’, *J. Chem. Theory Comput.*, vol. 10, no. 2, pp. 676–690, Feb. 2014, doi: 10.1021/CT400617G/SUPPL_FILE/CT400617G_SI_002.TXT.

[76] P. J. Stansfeld and M. S. P. Sansom, ‘From coarse grained to atomistic: A serial multiscale approach to membrane protein simulations’, *J. Chem. Theory Comput.*, vol. 7, no. 4, pp. 1157–1166, Apr. 2011, doi: 10.1021/CT100569Y/SUPPL_FILE/CT100569Y_SI_001.PDF.

[77] S. Rao, G. T. Bates, C. R. Matthews, T. D. Newport, O. N. Vickery, and P. J. Stansfeld, ‘Characterizing Membrane Association and Periplasmic Transfer of Bacterial Lipoproteins through Molecular Dynamics Simulations’, *Structure*, vol. 28, no. 4, pp. 475-487.e3, Apr. 2020, doi: 10.1016/J.STR.2020.01.012.

[78] M. G. Wolf, M. Hoefling, C. Aponte-SantamaríA, H. Grubmüller, and G. Groenhof, ‘g_membed: Efficient insertion of a membrane protein into an equilibrated lipid bilayer with minimal perturbation’, *J. Comput. Chem.*, vol. 31, no. 11, pp. 2169–2174, Aug. 2010, doi: 10.1002/JCC.21507.

[79] C. Kandt, W. L. Ash, and D. Peter Tieleman, ‘Setting up and running molecular dynamics simulations of membrane proteins’, *Methods*, vol. 41, no. 4, pp. 475–488, Apr. 2007, doi: 10.1016/J.YMETH.2006.08.006.

[80] E. Jefferys, Z. A. Sands, J. Shi, M. S. P. Sansom, and P. W. Fowler, ‘Alchembed: A Computational Method for Incorporating Multiple Proteins into Complex Lipid Geometries’, *J. Chem. Theory Comput.*, vol. 11, no. 6, pp. 2743–2754, Jun. 2015, doi: 10.1021/CT501111D/SUPPL_FILE/CT501111D_SI_002.ZIP.

[81] J. Yang, I. Anishchenko, H. Park, Z. Peng, S. Ovchinnikov, and D. Baker, ‘Improved protein structure prediction using predicted interresidue orientations’, *Proc. Natl. Acad. Sci. U. S. A.*, vol. 117, no. 3, pp. 1496–1503, Jan. 2020, doi: 10.1073/PNAS.1914677117/SUPPL_FILE/PNAS.1914677117.SAPP.PDF.

[82] H. M. Berman *et al.*, ‘The Protein Data Bank’, *Nucleic Acids Res.*, vol. 28, no. 1, pp. 235–242, Jan. 2000, doi: 10.1093/NAR/28.1.235.

[83] G. Madhavi Sastry, M. Adzhigirey, T. Day, R. Annabhimoju, and W. Sherman, ‘Protein and ligand preparation: Parameters, protocols, and influence on virtual screening enrichments’, *J. Comput. Aided. Mol. Des.*, vol. 27, no. 3, pp. 221–234, Apr. 2013, doi: 10.1007/S10822-013-9644-8/TABLES/9.

[84] A. L. Lomize, S. C. Todd, and I. D. Pogozheva, 'Spatial arrangement of proteins in planar and curved membranes by PPM 3.0', *Protein Sci.*, vol. 31, no. 1, pp. 209–220, Jan. 2022, doi: 10.1002/PRO.4219.

[85] P. C. Hsu *et al.*, 'CHARMM-GUI Martini Maker for modeling and simulation of complex bacterial membranes with lipopolysaccharides', *J. Comput. Chem.*, vol. 38, no. 27, pp. 2354–2363, Oct. 2017, doi: 10.1002/JCC.24895.

[86] Y. Qi, H. I. Ingólfsson, X. Cheng, J. Lee, S. J. Marrink, and W. Im, 'CHARMM-GUI Martini Maker for Coarse-Grained Simulations with the Martini Force Field', *J. Chem. Theory Comput.*, vol. 11, no. 9, pp. 4486–4494, Sep. 2015, doi: 10.1021/ACS.JCTC.5B00513/SUPPL_FILE/CT5B00513_SI_001.PDF.

[87] A. T. Boags, F. Samsudin, and S. Khalid, 'Binding from Both Sides: TolR and Full-Length OmpA Bind and Maintain the Local Structure of the E. coli Cell Wall', *Structure*, vol. 27, no. 4, pp. 713-724.e2, Apr. 2019, doi: 10.1016/J.STR.2019.01.001.

[88] D. H. De Jong *et al.*, 'Improved parameters for the martini coarse-grained protein force field', *J. Chem. Theory Comput.*, vol. 9, no. 1, pp. 687–697, Jan. 2013, doi: 10.1021/CT300646G/SUPPL_FILE/CT300646G_SI_001.PDF.

[89] X. Periole, M. Cavalli, S. J. Marrink, and M. A. Ceruso, 'Combining an elastic network with a coarse-grained molecular force field: Structure, dynamics, and intermolecular recognition', *J. Chem. Theory Comput.*, vol. 5, no. 9, pp. 2531–2543, Sep. 2009, doi: 10.1021/CT9002114/SUPPL_FILE/CT9002114_SI_001.PDF.

[90] S. O. Yesylevskyy, L. V. Schäfer, D. Sengupta, and S. J. Marrink, 'Polarizable Water Model for the Coarse-Grained MARTINI Force Field', *PLOS Comput. Biol.*, vol. 6, no. 6, p. e1000810, 2010, doi: 10.1371/JOURNAL.PCBI.1000810.

[91] M. J. Abraham *et al.*, 'GROMACS: High performance molecular simulations through multi-level parallelism from laptops to supercomputers', *SoftwareX*, vol. 1–2, pp. 19–25, Sep. 2015, doi: 10.1016/J.SOFTX.2015.06.001.

[92] W. Humphrey, A. Dalke, and K. Schulten, 'VMD: Visual molecular dynamics', *J. Mol. Graph.*, vol. 14, no. 1, pp. 33–38, Feb. 1996, doi: 10.1016/0263-7855(96)00018-5.

[93] J. Wang, A. Jain, L. R. McDonald, C. Gambogi, A. L. Lee, and N. V. Dokholyan, 'Mapping allosteric communications within individual proteins', *Nat. Commun. 2020 111*, vol. 11, no. 1, pp. 1–13, Jul. 2020, doi: 10.1038/s41467-020-17618-2.

[94] N. V. Dokholyan, 'Controlling Allosteric Networks in Proteins', *Chem. Rev.*, vol. 116, no. 11, pp. 6463–6487, Jun. 2016, doi: 10.1021/ACS.CHEMREV.5B00544/ASSET/IMAGES/MEDIUM/CR-2015-00544J_0017.GIF.

[95] S. Kim *et al.*, 'PubChem in 2021: new data content and improved web interfaces', *Nucleic Acids Res.*, vol. 49, no. D1, pp. D1388–D1395, Jan. 2021, doi: 10.1093/NAR/GKAA971.

[96] K. Zhu *et al.*, 'Docking covalent inhibitors: A parameter free approach to pose

prediction and scoring', *J. Chem. Inf. Model.*, vol. 54, no. 7, pp. 1932–1940, Jul. 2014, doi: 10.1021/CI500118S/SUPPL_FILE/CI500118S_SI_001.PDF.

[97] E. Sauvage *et al.*, 'Crystal Structure of Penicillin-Binding Protein 3 (PBP3) from Escherichia coli', *PLoS One*, vol. 9, no. 5, p. e98042, May 2014, doi: 10.1371/JOURNAL.PONE.0098042.

[98] M. A. Welsh, K. Schaefer, A. Taguchi, D. Kahne, and S. Walker, 'Direction of Chain Growth and Substrate Preferences of Shape, Elongation, Division, and Sporulation-Family Peptidoglycan Glycosyltransferases', *J. Am. Chem. Soc.*, vol. 141, no. 33, pp. 12994–12997, Aug. 2019, doi: 10.1021/JACS.9B06358/SUPPL_FILE/JA9B06358_SI_001.PDF.

[99] M. A. A. Ibrahim *et al.*, 'Non-β-lactam allosteric inhibitors target methicillin-resistant staphylococcus aureus: An in silico drug discovery study', *Antibiotics*, vol. 10, no. 8, p. 934, Aug. 2021, doi: 10.3390/ANTIBIOTICS10080934/S1.

[100] C. Contreras-Martel *et al.*, 'Molecular architecture of the PBP2–MreC core bacterial cell wall synthesis complex', *Nat. Commun. 2017 81*, vol. 8, no. 1, pp. 1–10, Oct. 2017, doi: 10.1038/s41467-017-00783-2.

[101] C. J. Murray *et al.*, 'Global burden of bacterial antimicrobial resistance in 2019: a systematic analysis', *Lancet*, vol. 399, no. 10325, pp. 629–655, Feb. 2022, doi: 10.1016/S0140-6736(21)02724-0.

CURRICULUM VITAE

Name Surname : Almotasem Belah Alhamwi

EDUCATION:

B.Sc. : 2021, Istanbul Medipol University,
School of Engineering and Natural Sciences,
Biomedical Engineering.

M.Sc. (If exists) : 2023, Istanbul Medipol University,
Graduate School of Engineering and Natural Sciences,
Biomedical Engineering and Bioinformatics.

PROFESSIONAL EXPERIENCE AND REWARDS:

- 2018, Intern at the biomedical engineering department of Medipol Mega hospital
- 2019, Intern at Sabanci University, faculty of engineering and natural sciences
- 2020, Undergraduate Teaching Assistance (TA), Istanbul Medipol University, Medical Biology course
- 2020 - 2023, Graduate Research Assistance (RA), SENSOY's computational biophysics lab, Istanbul Medipol University
- 2020 - 2023, Graduate Teaching Assistance (TA), Istanbul Medipol University, Medical Biology, Cellular and Molecular Biology, and Biochemistry courses

PUBLICATIONS, PRESENTATIONS, AND PATENTS ON THE THESIS:

- A. Alhamwi, C. Atılgan, and O. Sensoy, "Insight Into Impact of High Resistance Causing Mutations on Penicillin Binding Protein 3 of *H. influenzae* Suggests an Alternative Approach for Combating Antibiotic Resistance," *15th International Symposium on Health Informatics and Bioinformatics HIBIT'22 (20-22 October 2022),* 2022.
- A. Alhamwi, C. Atılgan, and O. Sensoy, "Insight Into Impact of High Resistance Causing Mutations on Penicillin Binding Protein 3 of *H. influenzae* Suggests an Alternative Approach for Combating Antibiotic Resistance," *ISCB-Latin America SoIBio BioNetMX Conference on Bioinformatics 2022 (03-07 November 2022),* 2022.

NON-LOCAL EFFECTS OF ANTIBIOTIC-RESISTANCE CAUSING MUTATIONS REVEAL AN ALTERNATIVE REGION FOR TARGETING ON FTSW/PENICILLIN BINDING PROTEIN 3 COMPLEX OF H. INFLUENZAE

ORIGINALITY REPORT

13%	10%	8%	3%
SIMILARITY INDEX	INTERNET SOURCES	PUBLICATIONS	STUDENT PAPERS

PRIMARY SOURCES

1	acikerisim.medipol.edu.tr Internet Source	2%
2	sens.medipol.edu.tr Internet Source	1%
3	elifesciences.org Internet Source	<1%
4	acikbilim.yok.gov.tr Internet Source	<1%
5	Asmaa Samy, Baris Suzek, Mehmet Ozdemir, Ozge Sensoy. "In Silico Analysis of a Highly Mutated Gene in Cancer Provides Insight into Abnormal mRNA Splicing: Splicing Factor 3B Subunit 1K700E Mutant", Biomolecules, 2020 Publication	<1%
6	link.springer.com Internet Source	<1%